Cellular/Molecular

# Subcellular Arrangement of Molecules for 2-Arachidonoyl-Glycerol-Mediated Retrograde Signaling and Its Physiological Contribution to Synaptic Modulation in the Striatum

**Motokazu Uchigashima,[1]* Madoka Narushima,[2,3]* Masahiro Fukaya,[1] Istvan Katona,[4] Masanobu Kano,[2] and Masahiko Watanabe[1]**

[1]Department of Anatomy, Hokkaido University School of Medicine, Sapporo 060-8638, Japan, [2]Department of Cellular Neuroscience, Graduate School of Medical Science, Osaka University, Suita 565-0871, Japan, [3]Core Research for Evolutional Science and Technology, Japan Science and Technology Agency, Tokyo 102-8666, Japan, and [4]Institute of Experimental Medicine, Hungarian Academy of Sciences, Szigony utca 43, 1083 Budapest, Hungary.

**Endogenous cannabinoids (endocannabinoids) mediate retrograde signals for short- and long-term suppression of transmitter release at synapses of striatal medium spiny (MS) neurons. An endocannabinoid, 2-arachidonoyl-glycerol (2-AG), is synthesized from diacylglycerol (DAG) after membrane depolarization and Gq-coupled receptor activation. To understand 2-AG-mediated retrograde signaling in the striatum, we determined precise subcellular distributions of the synthetic enzyme of 2-AG, DAG lipase-$\alpha$ (DAGL$\alpha$), and its upstream metabotropic glutamate receptor 5 (mGluR5) and muscarinic acetylcholine receptor 1 ($M_1$). DAGL$\alpha$, mGluR5, and $M_1$ were all richly distributed on the somatodendritic surface of MS neurons, but their subcellular distributions were different. Although mGluR5 and DAGL$\alpha$ levels were highest in spines and accumulated in the perisynaptic region, $M_1$ level was lowest in spines and was rather excluded from the mGluR5-rich perisynaptic region. These subcellular arrangements suggest that mGluR5 and $M_1$ might differentially affect endocannabinoid-mediated, depolarization-induced suppression of inhibition (DSI) and depolarization-induced suppression of excitation (DSE) in MS neurons. Indeed, mGluR5 activation enhanced both DSI and DSE, whereas $M_1$ activation enhanced DSI only. Importantly, DSI, DSE, and receptor-driven endocannabinoid-mediated suppression were all abolished by the DAG lipase inhibitor tetrahydrolipstatin, indicating 2-AG as the major endocannabinoid mediating retrograde suppression at excitatory and inhibitory synapses of MS neurons. Accordingly, $CB_1$ cannabinoid receptor, the main target of 2-AG, was present at high levels on GABAergic axon terminals of MS neurons and parvalbumin-positive interneurons and at low levels on excitatory corticostriatal afferents. Thus, endocannabinoid signaling molecules are arranged to modulate the excitability of the MS neuron effectively depending on cortical activity and cholinergic tone as measured by mGluR5 and $M_1$ receptors, respectively.**

*Key words:* **endocannabinoid; $CB_1$; 2-arachidonoyl-glycerol (2-AG); diacylglycerol lipase (DAGL); mGluR5; muscarinic acetylcholine receptor $M_1$; immunohistochemistry; striatum; mouse**

## Introduction

Endogenous cannabinoids (endocannabinoids) are released from postsynaptic neurons, act retrogradely on presynaptic $CB_1$ cannabinoid receptors, and cause short- and long-term suppression of transmitter release. Endocannabinoid-mediated retrograde suppression (ERS) was found originally in the hippocampus (Ohno-Shosaku et al., 2001; Wilson and Nicoll, 2001) and cerebellum (Kreitzer and Regehr, 2001; Maejima et al., 2001) and later in other brain regions (Chevaleyre et al., 2006; Hashimotodani et al., 2007). ERS can be triggered by membrane depolarization that elevates intracellular calcium concentration ($[Ca^{2+}]_i$) to a micromolar range (Brenowitz and Regehr, 2003; Maejima et al., 2005), activation of the Gq-protein-coupled metabotropic receptor/phospholipase C$\beta$ (PLC$\beta$) pathway leading to diacylglycerol (DAG) production (Maejima et al., 2001; Kim et al., 2002; Ohno-Shosaku et al., 2003), and their cooperative action (Varma et al., 2001; Ohno-Shosaku et al., 2002; Hashimotodani et al., 2005; Maejima et al., 2005). Of these, the third, cooperative mode appears physiologically the most relevant, because PLC$\beta$ serves as a coincidence detector of the two events and enables supralinear DAG production, even when either event is subthreshold for ERS by itself (Hashimotodani et al., 2005; Maejima et al., 2005; Ohno-Shosaku et al., 2005).

Received Jan. 31, 2007; revised Feb. 22, 2007; accepted Feb. 23, 2007.

This work was supported in part by grants-in-aid for Scientific Research on Priority Areas (17023001 to M.W.; 17023021 to M.K.), for Scientific Research (B) (17300108 to M.W.), and for Scientific Research (S) (17100004 to M.K.) from the Ministry of Education, Culture, Sports, Science, and Technology of Japan; by Hungarian Scientific Research Fund Grant F046407; and by Egészségügyi Tudományos Tanács Grant 561/2006 (I.K.). M.N. was a recipient of the Research Fellowship for Young Scientists from the Japan Society for the Promotion of Science (16-54131). I.K. is a grantee of the János Bolyai scholarship.

*M.U. and M.N. contributed equally to this work.

Correspondence should be addressed to Masahiko Watanabe, Department of Anatomy, Hokkaido University School of Medicine, Sapporo 060-8638, Japan. E-mail, watamasa@med.hokudai.ac.jp.

DOI:10.1523/JNEUROSCI.0448-07.2007

 0270-6474/07/273663-14$15.00/0

The striatum is the main input structure of the basal ganglia subserving motor and cognitive functions (Wilson, 2004). Medium spiny (MS) neurons are the principal neurons, whose activities are sculpted by extrastriatal activities of the sensorimotor cortex, thalamus, and substantia nigra and by GABAergic and cholinergic interneurons (Tepper and Bolam, 2004; Tepper et al., 2004). Excitatory and inhibitory synaptic responses onto MS neurons are sensitive to cannabinoid agonists (Szabo et al., 1998; Gerdeman and Lovinger, 2001; Huang et al., 2001). Moreover, ERS mediates both long-term depression (Gerdeman et al., 2002; Robbe et al., 2002; Ronesi et al., 2004; Kreitzer and Malenka, 2005; Ronesi and Lovinger, 2005; Wang et al., 2006) and short-term suppression at MS neuron synapses (Kreitzer and Malenka, 2005; Freiman et al., 2006; Narushima et al., 2006a,b, 2007; Yin and Lovinger, 2006). Importantly, striatal ERS is facilitated by activation of Gq-protein-coupled receptors, including group I metabotropic glutamate receptors (mGluRs) and $M_1$ muscarinic acetylcholine receptor (mAChR) (Kreitzer and Malenka, 2005; Freiman et al., 2006; Narushima et al., 2006a, 2007).

An endocannabinoid, 2-arachidonoyl-glycerol (2-AG), is synthesized on demand from DAG by *sn*-1-specific DAG lipase (Mechoulam et al., 1995; Sugiura et al., 1995; Stella et al., 1997; Bisogno et al., 2003). DAG lipase-$\alpha$ (DAGL$\alpha$) is targeted selectively to somatodendritic compartments and concentrated around spines (Katona et al., 2006; Yoshida et al., 2006), as is the case for group I mGluRs and PLC$\beta$ (Baude et al., 1993; Lujan et al., 1996; Nakamura et al., 2004; Mitrano and Smith, 2007). Indeed, DAG lipase inhibitors have been shown to abolish ERS in dopaminergic neurons and Purkinje cells (Melis et al., 2004; Safo and Regehr, 2005; Szabo et al., 2006). These findings together highlight 2-AG as a key mediator of ERS and thus prompted us to determine molecular, anatomical, and physiological bases of 2-AG-mediated ERS in the striatum.

## Materials and Methods

*Animal.* All experiments were performed according to the guidelines laid down by the animal welfare committees of Hokkaido University and Osaka University and by the United States National Institutes of Health Guide for the Care and Use of Laboratory Animals. Adult C57BL/6 mice and null-type gene knock-out mice lacking $CB_1$ (Zimmer et al., 1999) or mGluR5 (stock #003558; The Jackson Laboratory, Bar Harbor, ME) were used in the present study.

*Antibody.* We used affinity-purified primary antibodies raised against the following molecules (species immunized); mouse $CB_1$ (rabbit, guinea pig, and goat; see below), mouse DAGL$\alpha$ (rabbit and guinea pig) (Yoshida et al., 2006), rat mGluR5 (rabbit, guinea pig, and goat; see below), mouse mGluR1$\alpha$ (guinea pig) (Tanaka et al., 2000), mouse mAChR $M_1$ (rabbit) (Narushima et al., 2007), dopamine receptors $D_1$R (guinea pig and goat) (Narushima et al., 2006b) and $D_2$R (rabbit) (Narushima et al., 2006b), mouse microtubule-associated protein-2 (MAP2) (goat) (Miura et al., 2006), mouse parvalbumin (PV) (guinea pig and goat) (Nakamura et al., 2004; Miura et al., 2006), nitric oxide synthase (NOS) (rabbit) (Narushima et al., 2007), calretinin [rabbit (#7699/4); Swant, Bellinzona, Switzerland], substance P (SP) [rabbit (AB1566) and guinea pig (AB5892); Millipore, Billerica, MA], Leu-enkephalin (Enk) [rabbit (AB5024); Millipore], mouse vesicular glutamate transporters VGluT1 and VGluT2 (guinea pig and goat) (Miyazaki et al., 2003; Miura et al., 2006), mouse glutamic acid decarboxylase 65/67 (GAD) (rabbit) (Yamada et al., 2001), mouse vesicular GABA transporter (VGAT) (guinea pig and goat) (Miyazaki et al., 2003; Miura et al., 2006), mouse vesicular acetylcholine transporter (VAChT) (rabbit) (Nakamura et al., 2004), mouse plasmalemmal dopamine transporter (DAT) (rabbit, guinea pig, and goat; see below), mouse plasmalemmal serotonin transporter (HTT) (rabbit) (Somogyi et al., 2004), high affinity-choline transporter (CHT) (rabbit) (Narushima et al., 2007), and mouse plasmalemmal norepinephrine transporter (NET) (guinea pig and goat; see below).

For antibody production, cDNA fragments, which are preceded with a *Bam*HI site and encode C-terminal 28 aa of mGluR5 (amino acid residues 1144–1171; GenBank accession number D10891), N-terminal 60 aa of DAT (1–60; GenBank accession number BC054119), or N-terminal 56 aa of NET (1–56; GenBank accession number AY188506), were obtained by PCR using single-stranded mouse brain cDNA library. After the TA cloning using a pGEM-T Easy Vector System I kit (Promega, Madison, WI), cDNA fragments were sequenced and excised by *Bam*HI and *Eco*RI. These fragments were subcloned into pGEX4T-2 plasmid (GE Healthcare, Piscataway, NJ) for expression of glutathione *S*-transferase (GST) fusion proteins. GST fusion proteins were purified using glutathione–Sepharose 4B (GE Healthcare), according to the manufacturer's instructions. GST fusion proteins were emulsified with Freund's complete or incomplete adjuvant (DIFCO, Detroit, MI) and immunized subcutaneously to New Zealand White rabbits, Hartley guinea pigs, and goats at intervals of 2 weeks. After the sixth injection, Igs specific to antigens were affinity-purified using GST-free peptides coupled to CNBr-activated Sepharose 4B (GE Healthcare). GST-free peptides were prepared by in-column thrombin digestion of GST fusion proteins bound to glutathione-Sepharose 4B media. In the present study, $CB_1$ antibody was raised newly against the same antigen as used previously (Fukudome et al., 2004). The specificity of antibody and immunohistochemistry for DAGL$\alpha$ was confirmed by the disappearance of characteristic immunolabeling when using DAGL$\alpha$ antibody preabsorbed with the antigen, whereas that for mGluR5 and $CB_1$ was done by the lack of characteristic immunolabelings in the brains of knock-out mice (supplemental Fig. S1, available at www.jneurosci.org as supplemental material). The specificity of DAT and NET antibodies was confirmed in Western blots by selective detection of protein band at 60–65 or 45 kDa, respectively, and by selective neuronal labeling in the substantia nigra pars compacta or in the locus ceruleus, respectively (data not shown).

*Immunohistochemistry.* Under deep pentobarbital anesthesia (100 mg/kg body weight, i.p.), mice were fixed transcardially with 4% paraformaldehyde in 0.1 M sodium phosphate buffer (PB), pH 7.2, for light microscopy or 4% paraformaldehyde/0.1% glutaraldehyde in PB for electron microscopy. Thick sections (50 $\mu$m in thickness) were prepared by microslicer (VT1000S; Leica, Nussloch, Germany) and subjected to the free-floating method, whereas semithin cryosections (200 nm) were prepared by ultracryomicrotome (EM-FCS; Leica) and mounted on silane-coated glass slides.

All immunohistochemical incubations were done at room temperature. For immunofluorescence, microslicer sections and semithin cryosections were incubated successively with 10% normal donkey serum for 30 min, mixture of primary antibodies overnight (1 $\mu$g/ml), and mixture of Alexa 488-, indocarbocyanine (Cy3)-, and indodicarbocyanine (Cy5)-labeled species-specific secondary antibodies for 2 h at a dilution of 1:200 (Invitrogen, Eugene, OR; Jackson ImmunoResearch, West Grove, PA). Images were taken with a confocal laser-scanning microscope (FV1000; Olympus Optical, Tokyo, Japan).

For immunoperoxidase electron microscopy, microslicer sections were incubated successively with 10% normal donkey serum, primary antibodies (1 $\mu$g/ml), biotinylated secondary antibody, and streptavidin–peroxidase complex as above. Immunoreaction was visualized with 3,3′-diaminobenzidine. For preembedding immunogold electron microscopy, microslicer sections were dipped in 5% bovine serum albumin (BSA)/0.02% saponin/PBS for 30 min and incubated overnight with primary antibodies diluted with 1% BSA/0.004% saponin/PBS and then with secondary antibodies linked to 1.4 nm gold particles (Nanogold; Nanoprobes, Stony Brook, NY) for 2 h. Immunogolds were intensified with a silver enhancement kit (HQ silver; Nanoprobes). When combining the two methods for double immunoelectron microscopy, we executed both orders and confirmed essentially the same results. However, pictures shown in Figure 9*A–D* were taken from the specimens that had been subjected first to immunoperoxidase and then to immunogold, because this order prevented silver-enhanced immunogold particles from reductions in size and electron density. Sections labeled by immunoperoxidase and silver-enhanced immunogold were treated with 1%

osmium tetroxide for 15 min, stained in block with 2% uranyl acetate for 20 min, dehydrated, and embedded in Epon 812. Photographs were taken with an H-7100 electron microscope (Hitachi, Tokyo, Japan). For quantitative analysis, cell membrane-attached immunogold particles were counted on electron micrographs and analyzed using IPLab software (Nippon Roper, Tokyo, Japan). The mean number of membrane-attached gold particles/1 $\mu$m of plasma membrane was counted for each neuronal compartment (dendritic spine, dendritic shaft, soma, and axon). Statistical significance was assessed by Student's *t* test.

*Electrophysiology.* Coronal brain slices containing the cortex and the striatum (300 $\mu$m in thickness) were prepared from C57BL/6 mice aged to postnatal days 15–22 as described previously (Narushima et al., 2006a,b). Mice were decapitated under deep halothane anesthesia, and the brains were cooled in ice-cold, modified external solution containing the following (in mM): 120 choline-Cl, 2 KCl, 8 $MgCl_2$, 28 $NaHCO_3$, 1.25 $NaH_2PO_4$, and 20 glucose bubbling with 95% $O_2$ and 5% $CO_2$ (Narushima et al., 2006a,b). Slices were cut with Leica VT1000S slicer. For recovery, slices were incubated for at least 1 h in normal bathing solution composed of the following (in mM): 125 NaCl, 2.5 KCl, 2 $CaCl_2$, 1 $MgSO_4$, 1.25 $NaH_2PO_4$, 26 $NaHCO_3$, and 20 glucose, pH 7.4, which was bubbled continuously with a mixture of 95% $O_2$ and 5% $CO_2$ at room temperature. Whole-cell recordings were made from MS neurons in dorsolateral region of the striatum, using an upright microscope (BX50WI; Olympus Optical) equipped with infrared-CCD camera system (Hamamatsu Photonics, Hamamatsu, Japan) at 32°C. MS neurons were identified visually by their medium-sized, spherical somata. Resistance of the patch pipette was 3–5 M$\Omega$ when filled with the standard intracellular solution composed of the following (in mM): 50 CsCl, 90 Cs-gluconate, 10 HEPES, 1 EGTA, 0.1 $CaCl_2$, 4.6 $MgCl_2$, 4 Na-ATP, and 0.4 Na-GTP, pH 7.2, adjusted with CsOH. The pipette access resistance was compensated by 50–70%. MS neurons were usually held at a membrane potential of −80 mV. For recording EPSCs, the bath solution was supplemented with 20 $\mu$M (−)-bicuculline methochloride and 5 $\mu$M (*R*)-3-(2-carboxypiperazin-4-yl)-propyl-1-phosphonic [(*R*)-CPP; Tocris Bioscience, Bristol, UK]. Cortical EPSCs were evoked by stimulating white matter with bipolar platinum electrodes. For recording IPSCs, the bath solution was supplemented with 10 $\mu$M 2,3-dioxo-6-nitro-1,2,3,4-tetrahydrobenzo quinoxaline-7-sulfonamide (NBQX; Tocris Bioscience) and 5 $\mu$M (*R*)-CPP. Glass pipettes filled with normal saline were used to stimulate putative GABAergic fibers. Membrane currents were recorded with an EPC8 or EPC9 amplifier (HEKA Elektronik, Lambrecht/Pfalz, Germany). The PULSE software (HEKA Elektronik) was used for stimulation and data acquisition. The signals were filtered at 3 kHz and digitized at 20 kHz.

For testing effects of chemicals, two successive stimuli (duration, 0.1 ms; amplitude, 0–90 V) with an interstimulus interval of 50 ms were applied every 20 s. All drugs were bath applied. Effects of drugs were estimated as the percentage of the mean amplitudes of five consecutive IPSCs during drug application relative to that before application. In the experiments with tetrahydrolipstatin (THL), striatal slices were incubated with normal saline supplemented with 20 $\mu$M THL and 0.2 mg/ml BSA or BSA alone, for at least 1 h. Then the slice was moved to the recording chamber and was also superfused continuously with the external solution containing 10 $\mu$M THL during recording. Slices incubated with BSA alone were used as controls. Oxotremorine-M (oxo-M), (*RS*)-3,5-dihydroxyphenylglycine [(*RS*)-3,5-DHPG; DHPG] and (*R*)-(+)-[2,3-dihydro-5-methyl-3-(4-morpholinylmethyl)pyrrolo[1,2,3-de]-1,4-benzoxazin-6-yl]-1-naphthalenylmethanone mesylate (WIN 55,212-2) were purchased from Tocris Bioscience. BSA and THL were from Sigma-Aldrich (St. Louis, MO).

To induce depolarization-induced suppression of inhibition (DSI) or depolarization-induced suppression of excitation (DSE), a depolarizing pulse (0.1, 1, or 5 s duration from −80 to 0 mV) was applied to MS neurons. The magnitude of suppression was calculated as the percentage of reduction in the mean of three consecutive response amplitudes after depolarization relative to that of 10 consecutive response amplitudes just before depolarization. To quantify enhancement of DSI or DSE by some experimental manipulation, $\Delta$DSI or $\Delta$DSE was calculated by subtracting the DSI/DSE magnitude in the control condition from that after the experimental manipulation.

Averaged data from different experiments are presented as mean ± SEM. Statistical significance was assessed by Mann–Whitney *U* test (for comparison of two independent samples) or Wilcoxon signed rank test (for paired comparison of the same sample).

## Results

In the present study, 2-AG-mediated retrograde signaling was studied in the mouse striatum. All anatomical and physiological experiments were performed in the dorsolateral portion of the striatum, which is known to receive corticostriatal afferents from the sensorimotor cortex (Deniau et al., 1996; Ramanathan et al., 2002) and has the highest $CB_1$ expression level (Herkenham et al., 1991; Matsuda et al., 1993; Egertova and Elphick, 2000; Hohmann and Herkenham, 2000; Matyas et al., 2006).

### DAGL$\alpha$ is widely expressed on the somatodendritic surface of MS neurons with a distal-to-proximal gradient

To unravel the precise production site of 2-AG, we first examined the immunohistochemical localization of its synthetic enzyme DAGL$\alpha$ (Figs. 1, 2). DAGL$\alpha$ was distributed moderately throughout the striatum with higher distribution in the dorsolateral portion than in the remaining portions (supplemental Fig. S1*B*,*C*, available at www.jneurosci.org as supplemental material). Immunofluorescence at high magnifications visualized DAGL$\alpha$ as tiny puncta distributed on the surface of $D_1$R- and $D_2$R-positive bushy elements (Fig. 1*A1*,*A2*). The immunolabeled elements were judged mostly, if not all, to be somatodendritic neuronal elements, because DAGL$\alpha$ was preferentially distributed on the surface of MAP2-positive dendrites (Fig. 1*B1–C2*, arrows) and perikarya (Fig. 1*C1*,*C2*, arrowheads). Notably, the intensity of individual DAGL$\alpha$ puncta was apparently higher on $D_1$R-positive elements (Fig. 1*A1*,*A2*, asterisks) than on $D_2$R-positive ones (Fig. 1*A1*,*A2*, pound signs). In contrast, DAGL$\alpha$ showed no apparent overlap with glutamatergic terminal marker VGluT1 or inhibitory terminal marker VGAT but was distributed among these immunostained terminals (Fig. 1*D1*,*D2*). These results suggest that DAGL$\alpha$ is present as molecular clusters, which are distributed on the somatodendritic surface of the $D_1$R- and $D_2$R-positive MS neurons and are adjacent to both excitatory and inhibitory terminals. Furthermore, although we found no overlapping of DAGL$\alpha$ with the main target of 2-AG, the $CB_1$ cannabinoid receptor, this lipase was positioned very close to $CB_1$ (Fig. 1*E1*,*E2*).

This observation was verified and further characterized by immunoelectron microscopy (Fig. 2). Immunoperoxidase reaction products for DAGL$\alpha$ were observed as spotty deposition in spines, shafts of spiny dendrites, and somata with thin perikarya and round nuclei (Fig. 2*A*,*B*, open arrows). Using the silver-enhanced immunogold technique, metal particles representing DAGL$\alpha$ were detected on the cell membrane or around cytoplasmic vesicles in spines, dendritic shafts, and somata (Fig. 2*C–G*). On these somatodendritic elements, metal particles were found preferentially on the extrasynaptic membrane and were very rare on the postsynaptic membrane of asymmetrical (Fig. 2*C–E*, arrows) and symmetrical (Fig. 2*C*,*F*,*G*, arrowheads) synapses. To quantify more precisely this distribution pattern, the density of immunogold particles attached to the cell membrane was measured at the electron microscopic level. The density of DAGL$\alpha$ was highest in spines and decreased gradually toward somata (Fig. 2*H*). The density on the somatic membrane was three times lower than on the spine membrane but was even much higher

than on nerve terminals. Therefore, DAGLα is distributed widely on extrasynaptic somatodendritic surface of MS neurons in the order of spine > dendritic shaft > soma.

### Subcellular distribution of mGluR5 and DAGLα are similar to each other but different from mAChR $M_1$

Previous studies have shown that group I mGluR activation facilitates both DSI and DSE in MS neurons (Kreitzer and Malenka, 2005; Freiman et al., 2006; Narushima et al., 2006a). Our finding on the abundant DAGLα localization in spines prompted us to scrutinize the precise distribution of these receptors (mGluR1 and mGluR5) in the striatum in relation to DAGLα localization. In the forebrain, the striatum has the lowest level of mGluR1α immunostaining (supplemental Fig. S2*A*, available at www.jneurosci.org as supplemental material) but the highest level of mGluR5 immunostaining (supplemental Fig. S1*E*,*F*, available at www.jneurosci.org as supplemental material). Experiments with cell-type-specific neuronal markers revealed that this is attributable to the very low or to the very high expression of mGluR1α (supplemental Fig. S2*B–E*, available at www.jneurosci.org as supplemental material) or mGluR5 (see below), respectively, in MS neurons. Thus, mGluR5 is the major group I mGluR in MS neurons.

Similarly to DAGLα, mGluR5 was detected in both $D_1$R-positive and $D_2$R-positive elements (Fig. 3*A1*,*A2*), and was preferentially distributed on MAP2-positive dendrites (Fig. 3*B1–C2*, arrows) and perikarya (Fig. 3*C1*,*C2*, arrowheads). Different from DAGLα, however, no appreciable differences were discerned in the intensity of mGluR5 immunoreactivity between $D_1$R-positive and $D_2$R-positive elements (Fig. 3*A1*,*A2*). By silver-enhanced immunogold labeling, dense distribution of mGluR5 was demonstrated on the surface of spines, shafts of spiny dendrites, and somata of MS neurons (Fig. 3*D–G*). Precise quantification of high-resolution immunogold labeling revealed a decreasing density gradient in the order of spine > dendritic shaft > soma (Fig. 3*H*). The density in somata was twice as low as in spines, but was still much higher compared with nerve terminals. These results indicate that mGluR5 displays subcellular distribution similar to DAGLα in MS neurons.

$M_1$ muscarinic receptor is another Gq-coupled receptor expressed abundantly in MS neurons (Yan et al., 2001; Narushima et al., 2007), and its activation significantly enhances DSI (Narushima et al., 2007). We have recently shown that $M_1$ also displays widespread somatodendritic distribution in MS neurons, but its density is lower in spines than in dendritic shafts and somata (Narushima et al., 2007). In the present study, we compared their fine distribution on the spine head of MS neurons (Fig. 4). Wide extrasynaptic distribution in spines was common to both mGluR5 and $M_1$. However, mGluR5 tended to accumulate at the border between the postsynaptic density and the extrasynaptic membrane (0–40 nm from the edge of the synaptic junction) (Fig. 4*A*), whereas $M_1$ was rather low at this mGluR5-rich perisynaptic region (Fig. 4*B*). Therefore, mGluR5 is enriched in spines of MS neurons, particularly at the perisynaptic region, whereas $M_1$ is relatively sparse in spines and appears to be excluded from this perisynaptic region.

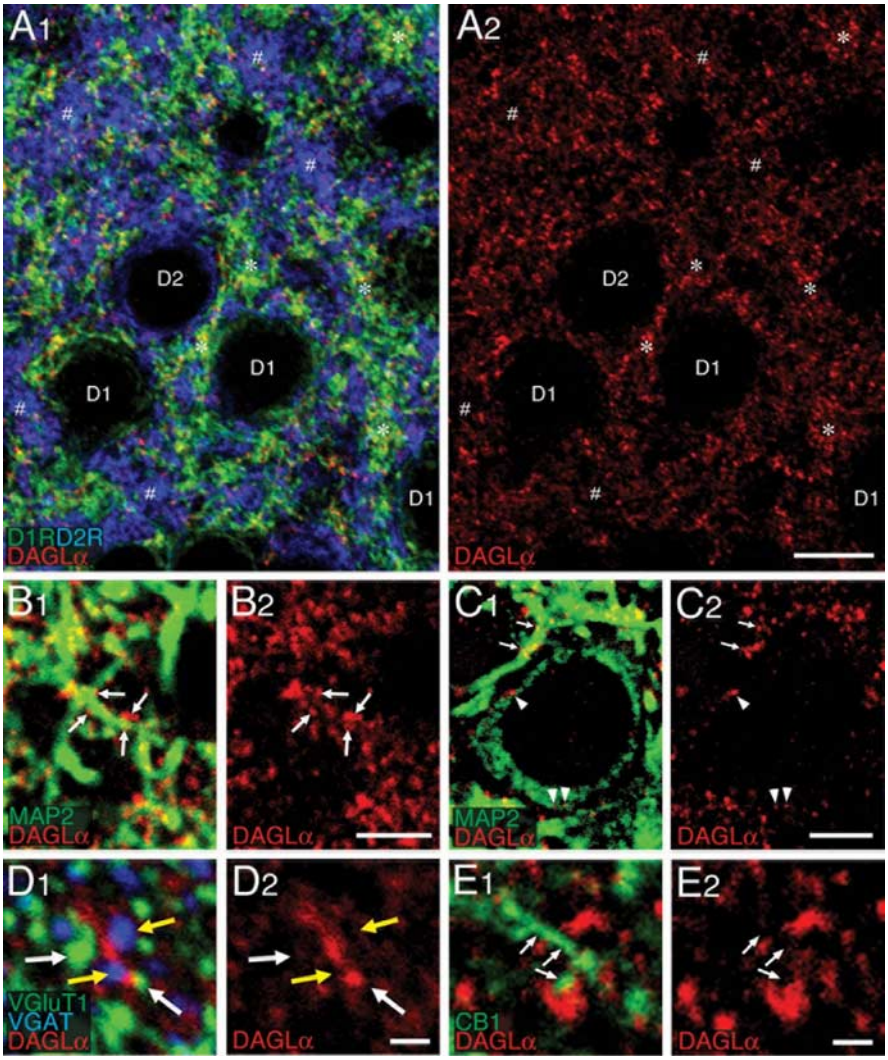


**Figure 1.** DAGLα is expressed on somatodendritic elements of $D_1$R-positive and $D_2$R-positive medium spiny neurons. Throughout this Figure, DAGLα is pseudocolored in red. ***A1***, ***A2***, Triple immunofluorescence for DAGLα, $D_1$R (green), and $D_2$R (blue). Note a punctate pattern of DAGLα immunolabeling, which is higher on $D_1$R-positive elements (*) than on $D_2$R-positive elements (#). ***B1– C2***, Double immunofluorescence for DAGLα and MAP2 (green). DAGLα is distributed on the surface of MAP2-positive dendrites (arrows) and perikarya (arrowheads). From thin perikaryal rim and round nucleus, the neuron in ***C1*** and ***C2*** is a putative MS neuron. ***D1***, ***D2***, Triple immunofluorescence for DAGLα, VGluT1 (green; white arrows), and VGAT (blue; yellow arrows). ***E1***, ***E2***, Double immunofluorescence for DAGLα and $CB_1$ (green; arrows). Scale bars: (in ***A2***) ***A1***, ***A2***, 10 μm; (in ***B2***, ***C2***) ***B1–C2***, 5 μm; (in ***D2***, ***E2***) ***D1–E2***, 1 μm.

### 2-AG is the major endocannabinoid for striatal DSI and DSE, and its release is facilitated by mGluR and/or mAChR activation

Strong depolarization of MS neurons triggers endocannabinoid-mediated suppression of striatal excitatory (Narushima et al., 2006a) and inhibitory (Narushima et al., 2006b) transmissions, and activation of $M_1$ mAChRs (Narushima et al., 2007) or group I mGluRs (Freiman et al., 2006; Narushima et al., 2006b) enhances this suppression. Considering that 2-AG is synthesized

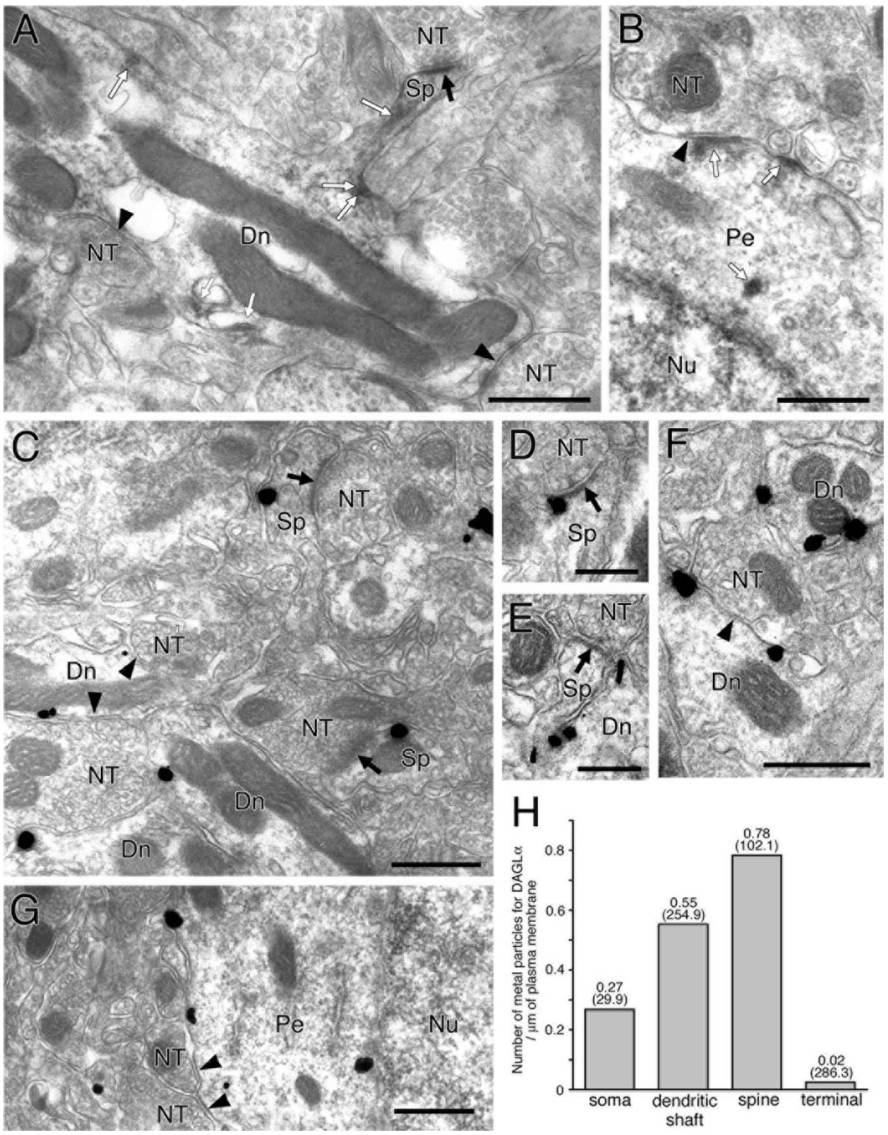


**Figure 2.** Immunoelectron microscopy demonstrating somatodendritic expression of DAGL$\alpha$ in spines, dendritic shafts, and somata of medium spiny neurons. Black arrows and arrowheads indicate asymmetrical or symmetrical synapses, respectively. ***A***, ***B***, Immunoperoxidase showing spotty labeling for DAGL$\alpha$ (open arrows) in spines (Sp), shaft dendrites (Dn), and perikarya (Pe) of presumed MS neurons. ***C–G***, Silver-enhanced immunogold showing preferential cell surface distribution of DAGL$\alpha$ in spine head and neck, shaft dendrites, and somata of presumed MS neurons. ***H***, The mean number of metal particles for DAGL$\alpha$ per 1 $\mu$m of the cell membrane. From very low density in nerve terminals, DAGL$\alpha$ is judged to be distributed selectively in somatodendritic compartments. Numbers in parentheses indicate the total length of measured cell membrane. NT, Nerve terminal; Nu, nucleus. Scale bars: ***A–C***, ***F***, ***G***, 500 nm; ***D***, ***E***, 250 nm.

from phosphatidylinositol by PLC$\beta$ and DAG lipase in an activity-dependent manner (Stella et al., 1997; Piomelli, 2003), 2-AG is likely to be synthesized after depolarization combined with activation of these Gq-coupled receptors and to act as an endocannabinoid at MS neuron synapses. To pursue this possibility, we examined the effect of the DAG lipase inhibitor tetrahydrolipstatin (THL) (Bisogno et al., 2003) on endocannabinoid-mediated modulations.

First, we tested THL on DSE or DSI. Bath application of THL (10 $\mu$M) after preincubation of slices with THL (20 $\mu$M) significantly blocked DSI induced by 5 s depolarization. The magnitude of DSI was 40.6 $\pm$ 4.6% in vehicle solution ($n = 6$), whereas it was 5.1 $\pm$ 1.0% in the presence of THL ($n = 8$, $p = 0.0019$) (Fig. 5*A*,*B*). Because Palomaki et al. (2007) have reported very recently that THL specifically antagonizes endocannabinoid-dependent $CB_1$ receptor activity, we tested whether THL has any effect on $CB_1$-induced suppression of IPSCs in MS neurons (supplemental Fig. S3, available at www.jneurosci.org as supplemental material). After we confirmed that the THL treatment abolished DSI, bath application of the cannabinoid agonist WIN 55,212-2 (1 $\mu$M) reduced the IPSC amplitude to 35.9 $\pm$ 4.7% ($n = 5$), which was not distinguishable from the suppression by WIN 55,212-2 in normal bathing solution (32.9 $\pm$ 3.6%; $n = 11$) (supplemental Fig. S3, available at www.jneurosci.org as supplemental material). Therefore, THL did not affect $CB_1$ receptor function in our experimental condition.

To induce discernible DSE of corticostriatal EPSCs, we combined 5 s depolarization of MS neurons with 50 $\mu$M DHPG, a group I mGluR agonist, because striatal DSE is observed only when long depolarization is combined with group I mGluR activation (Narushima et al., 2006a). This DHPG-enhanced DSE was also blocked by THL (magnitude of DSE, 29.5 $\pm$ 4.0% in vehicle solution, $n = 8$; 2.4 $\pm$ 4.3% in the presence of THL, $n = 6$, $p = 0.0019$) (Fig. 5*A*,*B*). Then, we examined THL on endocannabinoid-mediated synaptic suppression triggered by Gq-coupled receptor activation. For IPSCs, THL effectively blocked both DHPG-induced and the mAChR agonist oxo-M-induced suppressions (Fig. 5*C*,*D*). The averaged amplitude after DHPG or oxo-M application was 71.4 $\pm$ 6.0% ($n = 7$) or 56.5 $\pm$ 4.4% ($n = 6$) in vehicle-containing control solution, whereas the amplitude was 96.7 $\pm$ 1.7% ($n = 6$; $p = 0.0027$) or 91.2 $\pm$ 4.4% ($n = 7$; $p = 0.0027$) in THL. DHPG-induced suppression of corticostriatal EPSCs was also blocked by THL (averaged amplitude after DHPG application, 73.7 $\pm$ 2.4% in vehicle, $n = 7$; 100.8 $\pm$ 1.7% in THL, $n = 6$, $p = 0.0027$) (Fig. 5*E*,*F*). In contrast, THL had little effect on oxo-M-induced suppression of EPSCs (averaged amplitude after oxo-M application; 77.5 $\pm$ 4.1% in vehicle, $n = 6$; 81.5 $\pm$ 4.1% in THL, $n = 7$, $p = 0.57$). It has been shown that oxo-M-induced suppression of corticostriatal EPSC is mediated by presynaptic mAChR and is independent of $CB_1$ (Narushima et al., 2006a) (Fig. 5*E*,*F*). These results clearly indicate that postsynaptic depolarization, Gq-coupled receptor activation, and combined depolarization and Gq-coupled receptor activation all induce DAG lipase-mediated synthesis of 2-AG, which results in suppression of transmitter release at both GABAergic and glutamatergic synapses of MS neurons.

### DSE exhibits lower sensitivity to DHPG than DSI for enhancement

The different relative abundance of mGluR5 and $M_1$ on the somatodendritic surface and at the perisynaptic region suggests that these receptors may exhibit differential effects on 2-AG-mediated

suppression of glutamatergic and GABAergic synaptic transmission. Indeed, application of oxo-M can enhance DSI but not DSE (Narushima et al., 2006a) (Fig. 5*F*). However, DSE and DSI are both enhanced by DHPG (Freiman et al., 2006; Narushima et al., 2006a) (Fig. 5*C–F*), but their sensitivities to DHPG have not been compared quantitatively.

To address the aforementioned issue, the dose dependency of DSE/DSI enhancement on DHPG was compared by application of DHPG at concentration of 1, 5, or 25 $\mu$M, which treatment per se had little effect on the amplitude of IPSC or EPSC in MS neurons. DSI after 1 s depolarization was clearly enhanced by 1 or 5 $\mu$M DHPG (Fig. 6*A*,*C*). Similarly, DSI after 0.1 s depolarization was enhanced by 5 $\mu$M DHPG (Fig. 6*A*,*C*). Application of 1 or 5 $\mu$M DHPG, however, had little effect on DSE (Fig. 6*C*). When the concentration was raised to 25 $\mu$M, DHPG effectively enhanced both DSI ($n = 7$) and DSE ($n = 6$) (Fig. 6*B*). As summarized in Figure 6*C*, both DSI and DSE underwent dose-dependent enhancement by DHPG with the sensitivity of DSI being higher than that of DSE. It should be noted that no apparent enhancement was seen in DSI after 5 s depolarization, because DSI magnitude is saturated by 5 s depolarization (Narushima et al., 2007). These results indicate that DSE exhibits lower sensitivity to DHPG than DSI for enhancement.

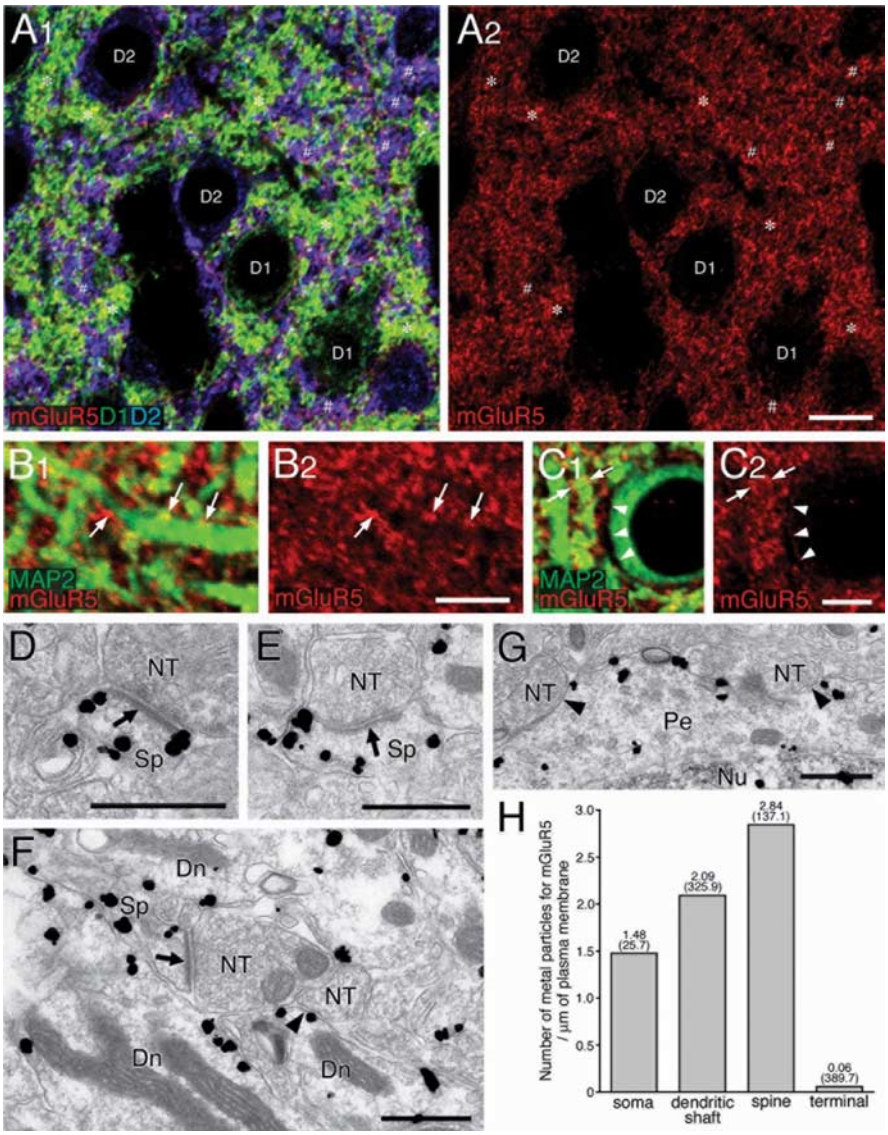


**Figure 3.** mGluR5 is distributed on somatodendritic elements of $D_1$R-positive and $D_2$R-positive medium spiny neurons. ***A1***, ***A2***, Triple immunofluorescence for mGluR5 (red), $D_1$R (green), and $D_2$R (blue). Note a punctate or reticular pattern of mGluR5 immunolabeling, which is detected on $D_1$R-positive (*) and $D_2$R-positive (#) elements in the neuropil. ***B1–C2***, Double immunofluorescence for mGluR5 (red) and MAP2 (green). In addition to dense mGluR5 labeling in the neuropil, low to moderate labeling can be detected on the surface of shaft dendrites (arrows) and somata (arrowheads) of presumed MS neurons. ***D–G***, Silver-enhanced immunogold showing preferential cell surface distribution of mGluR5 in spines (Sp), dendritic shafts (Dn), and perikarya (Pe) of presumed MS neurons. Arrows and arrowheads indicate asymmetrical and symmetrical synapses, respectively. NT, Nerve terminal; Nu, nucleus. ***H***, The mean number of metal particles for mGluR5 per 1 $\mu$m of the cell membrane. From very low density in terminals, mGluR5 is judged to be specific to somatodendritic compartments, similarly to DAGL$\alpha$. Numbers in parentheses indicate the total length of measured cell membrane. Scale bars: ***A2***, 10 $\mu$m; ***B2***, ***C2***, 2 $\mu$m; ***D–G***, 500 nm.

### DSE undergoes synergistic enhancement by coapplication of oxo-M and DHPG

Considering the wide distribution of $M_1$ and mGluR5 on the extrasynaptic spine surface (Fig. 4), these two receptors could potentially exert synergistic effects on DSE enhancement. To test this possibility, we examined cooperative effect of simultaneous activation of $M_1$ and mGluR5 on DSE. Application of subthreshold levels of DHPG alone (5 $\mu$M) or oxo-M alone (1 $\mu$M) could not enhance DSE after 5 s depolarization (summarized in Fig. 7*B*); the change in DSE magnitudes ($\Delta$DSE) after application of agonists was 4.0 $\pm$ 3.3% ($n = 6$) and 2.7 $\pm$ 2.1% ($n = 8$), respectively, showing no significant enhancement ($p = 0.35$ for DHPG, $p = 0.21$ for oxo-M; compared with DSE magnitude before application). In contrast, simultaneous application of 5 $\mu$M DHPG and 0.5 $\mu$M oxo-M clearly enhanced DSE as exemplified in Figure 7*A* and summarized in Figure 7*B* ($\Delta$DSE, 16.7 $\pm$ 2.0%, $n = 7$ vs DHPG alone, $p = 0.02$; vs oxo-M alone, $p = 0.0026$). The cooperative enhancement of DSE was effectively blocked by an $M_1$-preferring mAChR antagonist, pirenzepine (0.7 $\pm$ 2.3%; $n = 4$; $p = 0.0082$) (Fig. 7*B*). These findings indicate that group I mGluRs and $M_1$ act synergistically to facilitate endocannabinoid production in MS neurons.

### $CB_1$ cannabinoid receptor is highly expressed on two types of GABAergic axon terminals in the striatum

Our anatomical and physiological findings consistently indicate that 2-AG is the main endocannabinoid at both GABAergic and glutamatergic MS neuron synapses, except for the following point. Considering that spines are the postsynaptic targets of excitatory afferents (Fujiyama et al., 2004; Tepper et al., 2004), the lower sensitivity of DSE to DHPG than DSI for enhancement (Fig. 6) apparently contradicts the subcellular gradient of mGluR5 expression, being higher in spines than in dendritic

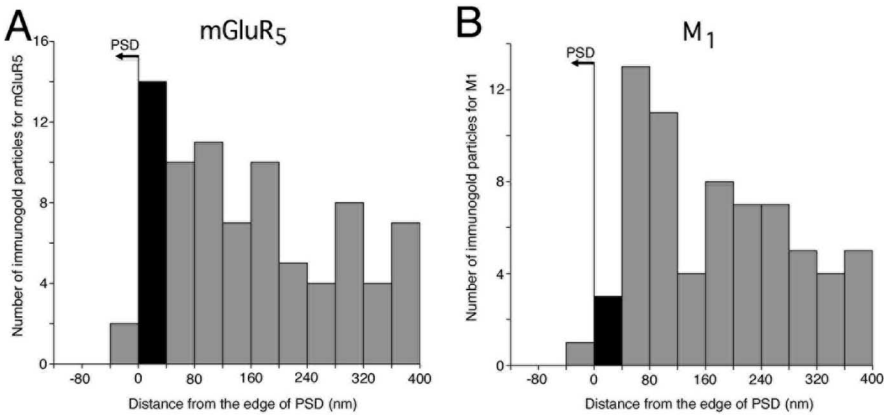


**Figure 4.** ***A***, ***B***, Histograms showing tangential distribution of cell membrane-associated immunogold particles for mGluR5 (***A***) and $M_1$ (***B***) on the spine head of medium spiny neurons. Immunoreaction was performed by preembedding silver-enhanced immunogold. The edge of postsynaptic density is defined as 0 with the synaptic and extrasynaptic side to the left and right, respectively. Note that the very perisynaptic region (0–40 nm bin, black columns) is provided with the highest labeling for mGluR5 but the lowest labeling for $M_1$ on the spine head. The total number of immunogold particles analyzed is 82 particles for mGluR5 and 69 particles for $M_1$. The total length of measured cell membrane is 36.0 $\mu$m for mGluR5 and 46.5 $\mu$m for $M_1$.

shafts and somata (Fig. 3). A possible solution to resolve this apparent discrepancy would be that the density of $CB_1$ might be different between excitatory and inhibitory afferents. We thus examined precise anatomical distribution of $CB_1$ in neural elements of the striatum. For this analysis, we used an antibody against the C-terminal segment of $CB_1$, whose specificity and sensitivity have been proven high enough to detect even a small amount of $CB_1$ proteins expressed in hippocampal excitatory afferents of wild-type but not of $CB_1$ knock-out mice (Fukudome et al., 2004; Katona et al., 2006; Kawamura et al., 2006).

By low-power observation over the forebrain, $CB_1$ was detected at moderate levels in the striatum (supplemental Fig. S1*H*,*I*, available at www.jneurosci.org as supplemental material). Its cellular and synaptic expression was determined by immunofluorescence (Fig. 8) and immunoelectron (Fig. 9) microscopies. At high magnification, intense $CB_1$ labeling was detected in large varicose fibers running throughout the neuropil (Fig. 8*A*′, arrows). Among these varicose fibers, thin structures with very faint $CB_1$ labeling were also seen (Fig. 8*A*′, arrowheads). In addition, faint labeling was observed in perikarya of various striatal neurons. To unravel the identity of these $CB_1$-immunoreactive profiles, we performed a series of double-immunofluorescence stainings in which neurochemical properties of these $CB_1$-carrying elements were characterized using transmitter-specific axon terminal markers and cell-type-specific perikaryal markers. For this analysis, semithin cryosections (200 nm in thickness) were prepared to increase the spatial resolution (Fig. 8*B–H*), and the specificity of $CB_1$ labeling was confirmed by using $CB_1$ knock-out semithin sections as negative controls (supplemental Fig. S4*A–G*, available at www.jneurosci.org as supplemental material).

First, we tested whether the swelling portions of varicose fibers having high levels of $CB_1$ (Fig. 8*A*′, arrows) belonged to GABAergic terminals. Many puncta labeled for inhibitory terminal marker VGAT were either positive for $CB_1$ or connected to $CB_1$-carrying fibers (Fig. 8*B1*,*B2*, arrowheads), whereas the rest of a few puncta were not associated with any $CB_1$ immunolabeling (Fig. 8*B1*,*B2*, arrow). This finding was further supported at the cellular level, as perikaryal $CB_1$ labeling was detected, although at low levels, in most of GAD-positive GABAergic perikarya inside the striatum (supplemental Fig. S4*H*, available at www.jneurosci.org as supplemental material). Next, we determined which types of GABAergic neurons expressed $CB_1$. Of striatal GABAergic neurons, two types of MS neurons are also distinguished by selective expressions of SP ($D_1$R neurons) and Enk ($D_2$R neurons), whereas three types of GABAergic interneurons are distinguished by selective expressions of PV, NOS/somatostatin (Som), and calretinin (CR). $CB_1$ was detected in SP-, Enk-, or PV-positive perikarya (Fig. 8*I1–K2*, arrows) and axons (Fig. 8*I1–K2*, arrowheads). Occasionally, $CB_1$ was discernible in NOS-positive interneurons, but the levels were extremely low, if any (supplemental Fig. S4*J*,*K*, available at www.jneurosci.org as supplemental material). No $CB_1$ immunostaining was seen in CR-containing interneurons (supplemental Fig. S4*L*, available at www.jneurosci.org as supplemental material). Therefore, among striatal GABAergic neurons, $CB_1$ is mainly expressed by MS neurons and PV-positive interneurons.

To confirm the presence of $CB_1$ on these GABAergic fibers, we prepared serial ultrathin sections subjected to double-labeling immunoelectron microscopy (Fig. 9*A1–D2*). The silver-enhanced immunogold method revealed that metal particles representing the precise subcellular localization of $CB_1$ were observed on terminals labeled by immunoperoxidase for either SP (Fig. 9*A1*,*A2*), Enk (Fig. 9*B1*,*B2*), or PV (Fig. 9*C1–D2*). Furthermore, these labeled terminals formed symmetrical contact (Fig. 9*A1–E*, arrowheads) on spines, spiny dendrites, and somata with thin perikaryal rims and round nuclei, all suggesting that their postsynaptic targets are MS neurons.

### $CB_1$ is expressed at low levels on glutamatergic axon terminals in the striatum

The very faint $CB_1$ immunolabeling in thin structures (Fig. 8*A*′, arrowheads) was also judged to be specific, because it was entirely missing in CB1 knock-out sections (supplemental Fig. S4*A–G*, available at www.jneurosci.org as supplemental material). To identify the structure, we performed double immunofluorescence staining using the following terminal markers: VGluT1 (glutamatergic terminal marker), VGluT2 (glutamatergic), VAChT (cholinergic), DAT (dopaminergic), HTT (serotonergic), and NET (norepinephrinergic) (Fig. 8*C1–H2*). Among these terminal markers, faint $CB_1$ labeling was often detected on VGluT1-positive terminals only (Fig. 1*D1*,*D2*). Considering that VGluT1 is selectively present in glutamatergic afferents from the sensorimotor cortex, whereas VGluT2-containing glutamatergic axons are derived from the parafascicular thalamic nucleus (Fujiyama et al., 2004), the above results suggest that $CB_1$ is expressed at low levels in corticostriatal glutamatergic afferents but not in other subcortical afferents. In support of this notion, moderate levels of $CB_1$ mRNA were detected in layer V neurons of the sensorimotor cortex, which send corticostriatal afferents (supplemental Fig. S5*C*,*D*, available at www.jneurosci.org as supplemental material). In contrast, $CB_1$ mRNA was at the background level, if any, in neurons of the parafascicular thalamic nucleus, substantia nigra pars compacta, dorsal raphe, and locus ceruleus, which supply glutamatergic, dopaminergic, serotonergic, and norepinephrinergic afferents, respectively, to the striatum (sup-

plemental Fig. S5*E–O*, available at www.jneurosci.org as supplemental material).

$CB_1$ expression in corticostriatal afferents was verified by immunogold labeling for $CB_1$. Metal particles representing the localization of $CB_1$ were indeed found on nerve terminals forming asymmetrical synapses onto dendritic spines (Fig. 9*E*, arrow). Quantification of metal particles on electron micrographs revealed that the density of $CB_1$-labeling was 3.6-fold higher on axon terminals forming symmetrical synapses than on boutons making asymmetrical synapses (Fig. 9*F*) ($p < 0.01$, Student's $t$ test). The labeling at asymmetrical synapses was judged to be specific, because the density was significantly higher than the control level as determined from the density at asymmetrical synapses of $CB_1$ knock-out mice (Fig. 9*F*) ($p < 0.01$).

Together, $CB_1$ cannabinoid receptor in the striatum is localized at high levels on GABAergic afferents forming PV interneuron–MS neuron (PV–MS) synapses and MS neuron collateral–MS neuron (MS–MS) synapses, as well as at low levels on glutamatergic afferents forming corticostriatal synapses.

## Discussion

Through molecular, anatomical, and physiological approaches, our findings highlight that the 2-AG-mediated retrograde signaling system is organized in the striatum in a highly regulated manner, as schematically illustrated in Figure 10.

### Comparison with previous studies on striatal $CB_1$ expression

High $CB_1$ expression on inhibitory axons/terminals of PV interneurons and MS neurons is compatible with previous studies using double-labeling *in situ* hybridization (Marsicano and Lutz, 1999; Hohmann and Herkenham, 2000) and with an immunogold study showing dense distribution of $CB_1$ on GABAergic axons and terminals in the striatum (Matyas et al., 2006). Low $CB_1$ immunoreactivity in NOS-positive interneurons (supplemental Fig. S4*J*,*K*, available at www.jneurosci.org as supplemental material) is not incompatible with negativity of $CB_1$ mRNA in Som-positive interneurons (Hohmann and Herkenham, 2000); rather, the two studies are consistent in that $CB_1$ expression in this interneuron is around the threshold level. Here we have further demonstrated that the $CB_1$-rich GABAergic elements are the afferents of PV–MS and MS–MS synapses and that $CB_1$ is also expressed on corticostriatal excitatory synapses. Importantly, these anatomical results are fully compatible with the electrophysiological findings that ERS is observed at PV–MS (Freiman et al., 2006; Narushima et al., 2006b), MS–MS (Freiman et al., 2006), and corticostriatal synapses (Gerdeman and Lovinger, 2001; Huang et al., 2001; Kreitzer and Malenka, 2005; Narushima et al., 2006a).

In contrast, our predominant CB1 staining in presynaptic elements is quite different from intense perikaryal staining of various striatal neurons, as shown by Fusco et al. (2004). Intense perikaryal labeling was reported for CCK-positive interneurons in the hippocampus, cerebral cortex, and amygdala (Katona et al., 1999, 2001; Hajos et al., 2000; Fukudome et al., 2004; Bodor et al., 2005) but has never been seen in the striatum (Julian et al., 2003; Matyas et al., 2006) (Fig. 8). The lack of $CB_1$ in the postsynaptic density and dopaminergic afferents in our study is also incom-

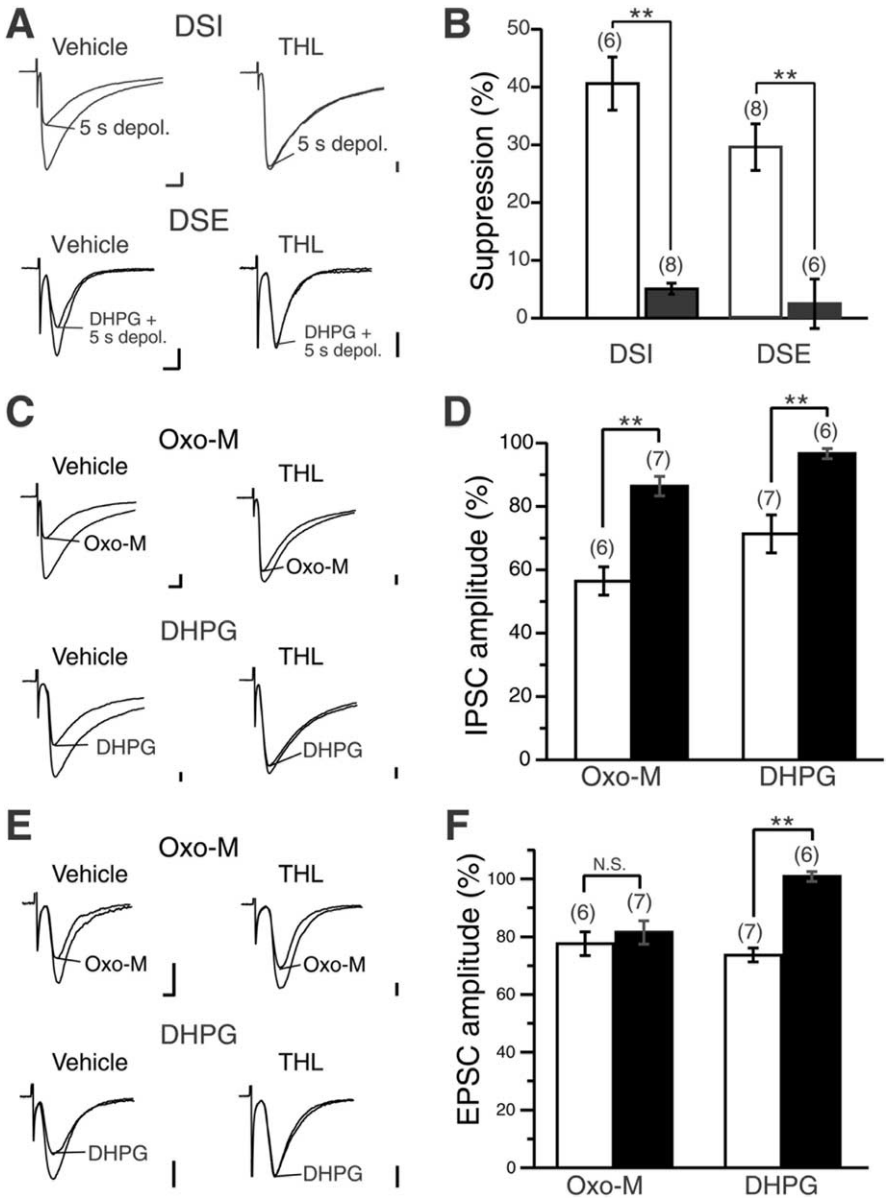


**Figure 5.** DAGL inhibitor prevents endocannabinoid-mediated retrograde signaling in the striatum. ***A***, Sample traces of IPSC (top) and EPSC (bottom) showing the suppression induced by 5 s depolarization (depol.) in vehicle solution (left) and in the presence of THL (right). For EPSC, 50 $\mu$M DHPG was supplemented to induce DSE. ***B***, Summary bar graph showing average magnitudes of DSI and DSE after 5 s depolarization in vehicle solution (open columns) and in the presence of THL (filled columns). ***C***, Sample traces showing the effect of 1 $\mu$M oxo-M or 50 $\mu$M DHPG on IPSCs recorded from MS neurons in the BSA-containing vehicle solution (vehicle) and in the presence of THL (THL). ***D***, Summary bar graph showing the suppression of IPSCs by oxo-M or DHPG. Data are expressed as a percentage of IPSC amplitudes in oxo-M or DHPG relative to the values before oxo-M or DHPG application in the vehicle solution (open columns) and in the presence of THL (filled columns). ***E***, Sample traces showing the effect of oxo-M and DHPG on EPSCs. ***F***, Summary bar graph showing the effect of oxo-M and DHPG on EPSCs. N.S., Not significant. Data are illustrated similarly to ***D***. Calibration: 100 pA, 5 ms. $^{**}p < 0.01$.

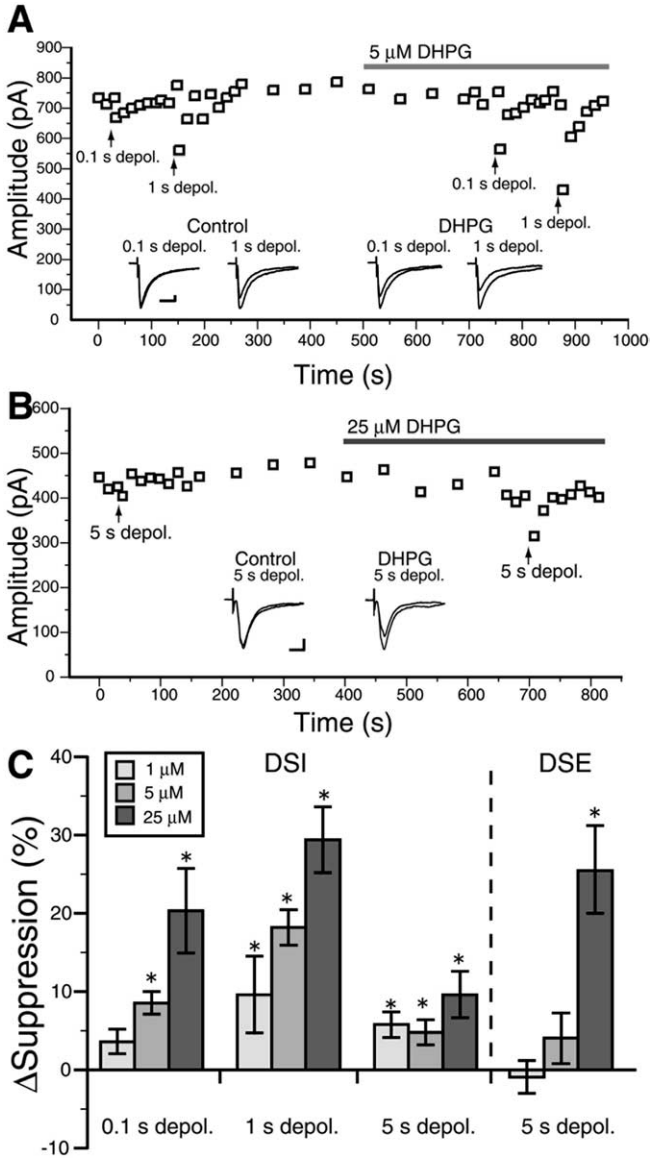


**Figure 6.** Activation of group I mGluRs causes dose-dependent enhancement of striatal DSI and DSE. ***A***, Representative data demonstrating enhancement of DSI by 5 $\mu$M DHPG. Each point represents the average of three consecutive traces. Depolarizing pulses (depol.) with duration of 0.1 or 1 s were applied before and during DHPG application at the time points indicated with upward arrows. Inset, Sample IPSC traces showing DSI in the control external solution and in the presence of 5 $\mu$M DHPG. Calibration: 100 pA, 10 ms. ***B***, Representative data demonstrating enhancement of DSE by 25 $\mu$M DHPG. Depolarizing pulses with 5 s duration were applied before and during DHPG application. Inset, Sample EPSC traces showing DSE before and after DHPG application. Calibration: 100 pA, 10 ms. ***C***, Summary bar graphs showing dose-dependent enhancement of DSI and DSE by DHPG. The degree of enhancement was calculated as the change in the magnitude of DSI or DSE during DHPG application relative to the value before application (ΔSuppression).

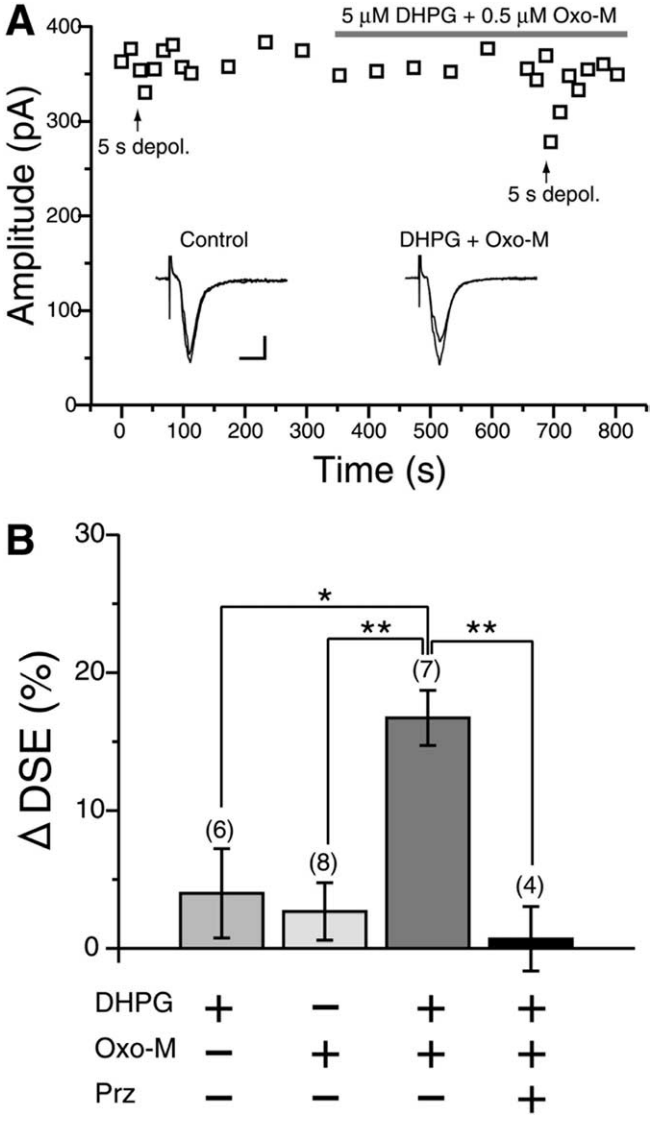


**Figure 7.** Cooperative enhancement of DSE by combined activation of $M_1$ and group I mGluRs. ***A***, Representative data showing enhancement of DSE by combined application of 5 $\mu$M DHPG and 0.5 $\mu$M oxo-M. Data are shown in a manner similar to Figure 6*B*. Calibration: 100 pA, 10 ms. depol., Depolarizing pulse. ***B***, Summary bar graph showing enhancement of DSE by 5 $\mu$M DHPG alone, 1 $\mu$M oxo-M alone, coapplication of 5 $\mu$M DHPG and 0.5 $\mu$M oxo-M, and coapplication of DHPG and oxo-M in the presence of 1 $\mu$M pirenzepine (Prz).

patible with the study by Kofalvi et al. (2005). Although reasons for these discrepancies remain unclear, we verified the specificity of our $CB_1$ immunohistochemistry by negative immunostaining in the $CB_1$-knock-out striatum (Fig. 9*F*, supplemental Figs. S1*H*, S4*A–G*, available at www.jneurosci.org as supplemental material).

### 2-AG-mediated retrograde suppression at corticostriatal synapse

In addition to $CB_1$ expression on corticostriatal afferents, we have revealed for the first time that DAGL$\alpha$ is distributed at the highest level on spines of MS neurons. As for mGluR5, our observations of somatodendritic distribution in the order of spine > dendritic shaft > soma, predominant extrasynaptic expression, and perisynaptic accumulation at asymmetrical synapses are consistent with previous studies (Paquet and Smith, 2003; Mitrano and Smith, 2007). This molecular organization will explain the electrophysiological findings that corticostriatal excitatory transmission is suppressed by $CB_1$ agonists (Gerdeman and Lovinger, 2001; Huang et al., 2001) and that DSE and endocannabinoid-dependent LTD are induced in MS neurons only when postsynaptic depolarization or L-type calcium channel activation is combined with group I mGluR activation (Kreitzer and Malenka, 2005; Narushima et al., 2006a) (Fig. 6). Such cooperativity is also found for hippocampal neurons (Varma et al., 2001; Ohno-Shosaku et al., 2002) and cerebellar Purkinje cells (Brenowitz and Regehr, 2005; Maejima et al., 2005). PLC$\beta$ is sensitive to both intracellular calcium levels and Gq activity and functions as a

coincidence detector of the two events (Hashimotodani et al., 2005; Maejima et al., 2005).

In awake animals, MS neurons are almost quiescent (i.e., down-state) when the animals are at rest. MS neurons display transient high-frequency firing (up-state) in response to synchronous excitatory inputs from the sensorimotor cortex, when the animals initiate movements (Hikosaka and Wurtz, 1989). As cortical activity is increased, high-frequency activation of ionotropic and metabotropic glutamate receptors activates PLC$\beta$ supralinearly (most likely PLC$\beta$1 in MS neurons) (Watanabe et al., 1998), elevates DAG levels in the activated spines, and produces 2-AG from DAG by DAGL$\alpha$. Then, 2-AG travels backwards to suppress glutamate release from the terminals (Fig. 10, right). Intriguingly, in slice preparation, DSE cannot be induced by depolarization alone and requires coactivation of group I mGluRs (Narushima et al., 2006a). Because $CB_1$ density is low on corticostriatal afferents, relatively high concentration of 2-AG around corticostriatal excitatory synapses must be required for DSE induction. The abundance of mGluR5 and DAGL$\alpha$ in spines should help 2-AG synthesis beyond the threshold, when postsynaptic depolarization and mGluR5 activation coincide. Hence, such molecular arrangements around corticostriatal synapses should enable this local feedback loop to operate only after robust cortical excitation, which leads to suppression of hyperactivity of the MS neuron.

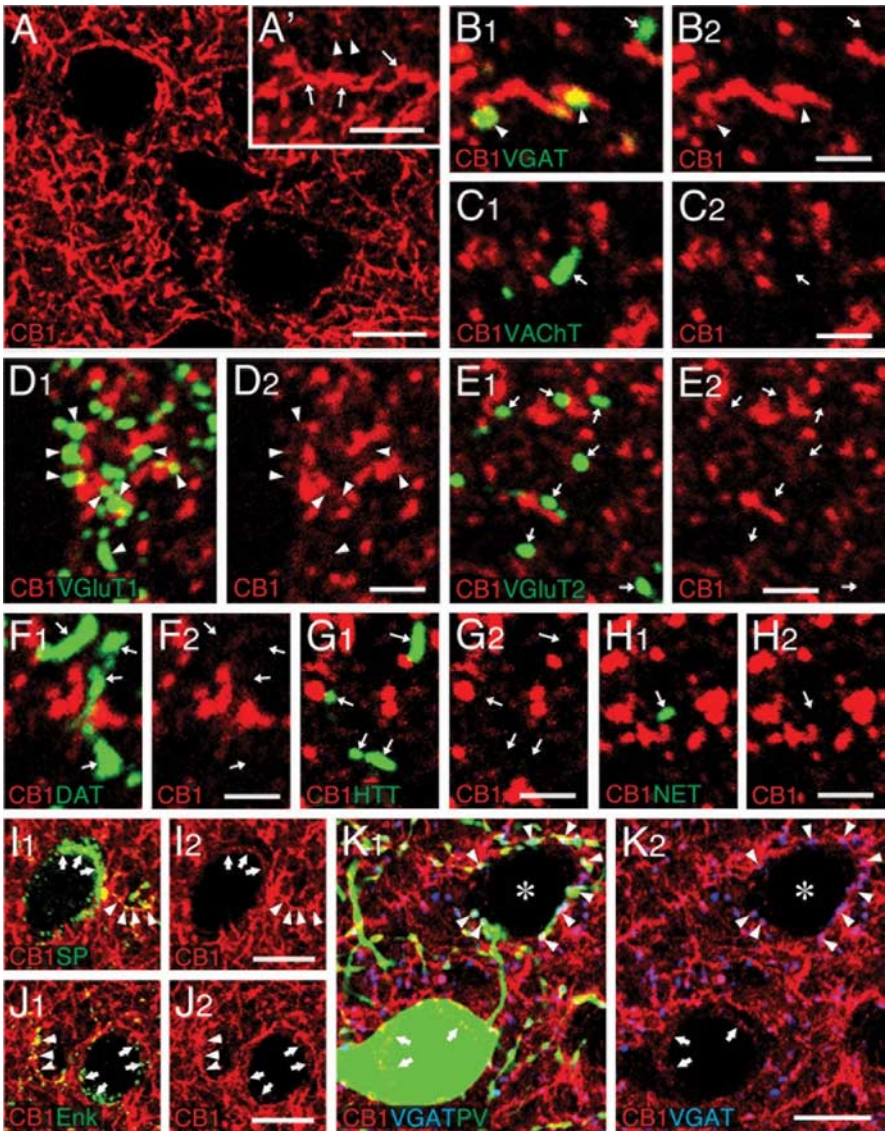


**Figure 8.** $CB_1$ is highly expressed in axons and terminals of medium spiny neurons and parvalbumin interneurons. Throughout this figure, $CB_1$ is pseudocolored in red. ***A***, Single immunofluorescence for $CB_1$. Inset, Arrows and arrowheads indicate intense (putative inhibitory afferents) and weak (putative excitatory afferents) $CB_1$ immunolabeling, respectively. ***B1–H2***, Semithin cryosections subjected to double immunofluorescence for $CB_1$ and terminal markers (green; ***B1***,***B2***, vesicular GABA transporter VGAT; ***C1***,***C2***, vesicular acetylcholine transporter VAChT; ***D1***,***D2***, type 1 vesicular glutamate transporter VGluT1; ***E1***,***E2***, type 2 vesicular glutamate transporter VGluT2; ***F1***,***F2***, plasmalemmal dopamine transporter DAT; ***G1***,***G2***, plasmalemmal serotonin transporter HTT; ***H1***,***H2***, plasmalemmal norepinephrine transporter NET). Arrowheads and arrows indicate terminals judged to be positive and negative for $CB_1$, respectively. ***I1–J2***, Double immunofluorescence for $CB_1$ and SP (green; ***I1***, ***I2***) or enkephalin (Enk) (green; ***J1***, ***J2***). Note low $CB_1$ contents in neuropeptide-carrying perikarya (arrows) and high $CB_1$ contents in neuropeptide-carrying axons (arrowheads). ***K1***, ***K2***, Triple immunofluorescence for $CB_1$, PV (green), and VGAT (blue). Note low $CB_1$ contents in PV-carrying perikarya (arrows) and high $CB_1$ contents in PV/VGAT-carrying terminals (arrowheads), the latter surrounding a putative MS neuron (asterisk) in a basket-like manner. Scale bars: ***A***, ***I2***, ***J2***, ***K2***, 10 $\mu$m; ***A′***, ***B2***, ***C2***, ***D2***, ***E2***, ***F2***, ***G2***, ***H2***, 2 $\mu$m.

### 2-AG-mediated retrograde suppression at PV–MS and MS–MS synapses

Inhibitory synaptic transmissions at PV–MS and MS–MS synapses are also sensitive to $CB_1$ agonists (Szabo et al., 1998; Freiman et al., 2006; Narushima et al., 2006b), and the magnitude of DSI is enhanced by activation of group I mGluRs (Freiman et al., 2006) (Fig. 5*C*,*D*). In contrast to DSE, DSI in MS neurons can be induced by depolarization alone (Narushima et al., 2006b). This may be relevant to abundant $CB_1$ at these inhibitory synapses. Moreover, robust DSI enhancement by activation of group I mGluRs or $M_1$ (Narushima et al., 2007) (Fig. 5*C–F*) and the distribution of DAGL$\alpha$, mGluR5, and $M_1$ around inhibitory synapses (Narushima et al., 2007) (Figs. 2, 3) point to the physiological importance of coincidental activation of these Gq-coupled receptors for DSI induction (Fig. 10, left), as is the case for DSE induction. Indeed, ambient acetylcholine derived from cholinergic interneurons is involved in tonic enhancement of DSI in MS neurons (Narushima et al., 2007).

PV or fast-spiking interneurons receive cortical excitatory inputs and exert powerful inhibition onto the MS neuron through their pericellular basket formation and through their electrical coupling via gap junction (Kita et al., 1990; Koos and Tepper, 1999; Bolam et al., 2000). Even a single spike of PV interneuron can delay or prevent spiking in an MS neuron (Koos and Tepper, 1999). Therefore, PV–MS synapse constitutes a powerful feedforward inhibitory circuits, and DSI at this synapse leads to the increase of the excitability of the MS neuron. On the other hand, MS neuron collaterals form numerous inhibitory synapses onto dendritic shafts and spines of MS neurons (Kubota and Kawaguchi, 2000; Wilson, 2004). Compared with PV–MS synapses, MS–MS synapses produce smaller IPSCs when measured at the

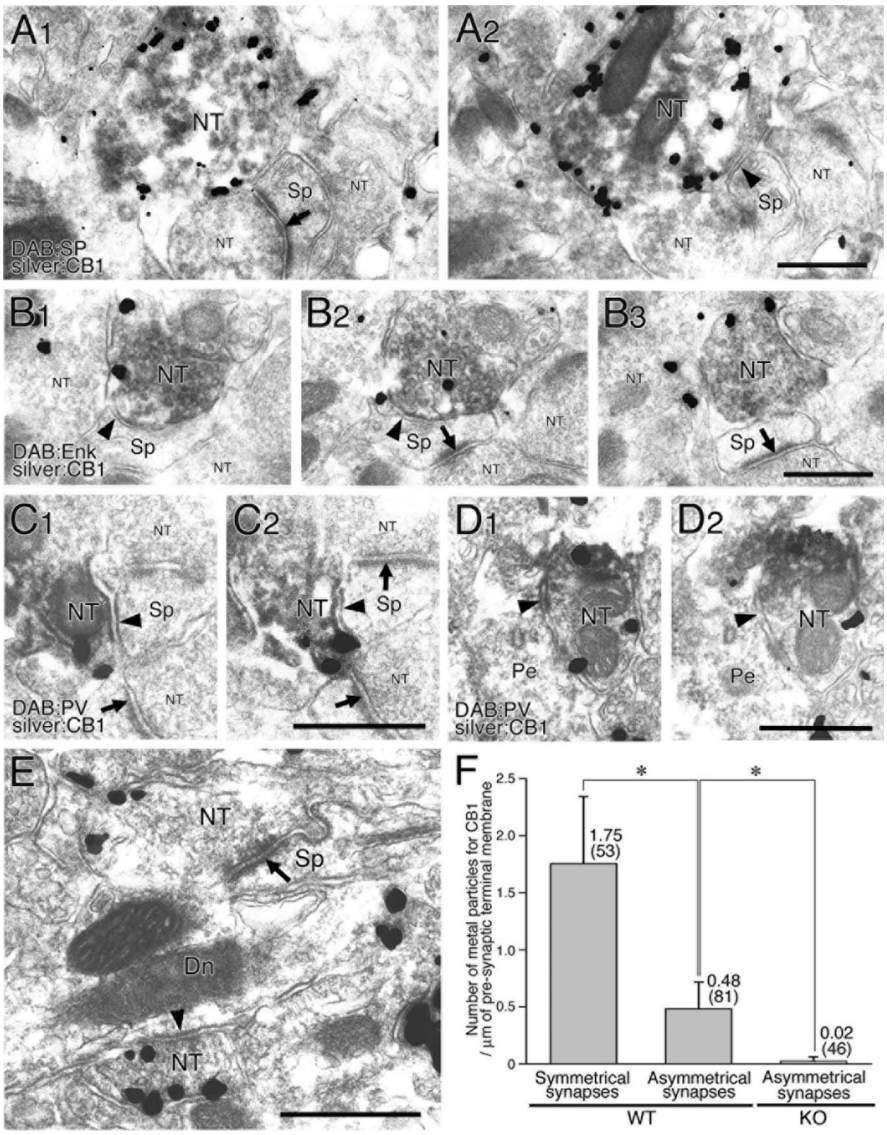


**Figure 9.** Immunoelectron microscopy demonstrating dense $CB_1$ localization in axons and terminals of MS neurons and PV interneurons. ***A1–D2***, Double labeling by preembedding silver-enhanced immunogold for $CB_1$ and immunoperoxidase for neuronal markers (***A1***, ***A2***, SP; ***B1–B3***, Enk; ***C1–D2***, PV). Note the dense $CB_1$ labeling on the cell membrane of SP-, Enk-, or PV-positive nerve terminals (NT in larger font), all forming symmetrical synapses (arrowheads) onto dendritic spines (Sp) or perikarya (Pe). Arrows indicate asymmetrical synapses, whose presynaptic nerve terminals are rarely labeled by double-labeling experiment, because of lower sensitivity than single immunogold labeling. Two or three consecutive images from serial sections show reproducible immunogold labeling on the terminal membrane. ***E***, Single immunogold labeling for $CB_1$. Low but significant labeling can be detected on the terminal membrane (top left portion; NT) forming an asymmetrical synapse (arrow) with an MS neuron spine. See heavy labeling on a nerve terminal forming a symmetrical synapse (arrowhead) with a dendritic shaft (Dn). ***F***, The mean number of metal particles per 1 $\mu$m of presynaptic terminal membrane. $CB_1$ labeling is 3.6 times higher at symmetrical synapses than at asymmetrical synapses in wild-type (WT) control mice. The background level is determined from labeling density at asymmetrical synapses of $CB_1$ knock-out (KO) mice. Numbers in parentheses indicate the number of synaptic profiles examined. The total length of measured cell membrane is 101.7 $\mu$m for symmetrical synapses in wild-type mice, 140.3 $\mu$m for asymmetrical synapses in wild-type mice, and 81.2 $\mu$m for asymmetrical synapses in $CB_1$ knock-out mice. Error bars indicate the mean $\pm$ SD. $^*p < 0.01$. Scale bars, 500 nm.

soma and are thought to modulate dendritic integration and synaptic plasticity of corticostriatal and thalamostriatal synapses and to attenuate backpropagation of action potentials into dendrites (Tepper et al., 2004). Therefore, DSI of MS–MS synapse may augment excitability of the MS neuron less effectively than that of PV–MS synapse but would elaborate on information processing in local dendrites of MS neurons.

### Differential but synergistic modulation by glutamatergic and cholinergic inputs on DSE enhancement

Although group I mGluR agonist DHPG enhances both DSI and DSE, mAChR agonist oxo-M enhances DSI only (Narushima et al., 2006a) (Fig. 5*C–F*). However, oxo-M can readily enhance DSE when coadministered with DHPG (Fig. 7). This finding suggests that induction threshold for striatal ERS is modulated differentially but synergistically depending on cholinergic and cortical activities. Tonically active cholinergic interneurons in primates change their firings in response to reward-related or aversive stimuli (Apicella, 2002). Cholinergic interneuron activity is also influenced by nigrostriatal dopaminergic and thalamostriatal glutamatergic inputs (Aosaki et al., 1994; Bennett and Wilson, 1998; Watanabe and Kimura, 1998). Therefore, it can be assumed that as cholinergic activity is elevated alone, the threshold for DSI decreases preferentially, whereas that for both DSI and DSE decreases when cholinergic and corticostriatal activities are elevated simultaneously. Thus, the balance between cholinergic and cortical inputs will determine the degree of ERS of inhibition and excitation and should modulate striatal output.

In hippocampal pyramidal cells and Purkinje cells, mGluR1$\alpha$ and mGluR5 are accumulated at the perisynaptic annulus of excitatory synapses (Baude et al., 1993; Nusser et al., 1994; Lujan et al., 1996, 1997). These group I mGluRs form complexes coimmunoprecipitated with inositol 1,4,5-trisphosphate receptor (IP3R) via scaffolding protein Homer (Brakeman et al., 1997; Tu et al., 1998). Homer further binds to ionotropic glutamate receptors via Shank and GRIP (glutamate receptor-interacting protein) (Dong et al., 1997; Sheng and Kim, 2000; Uemura et al., 2004). Furthermore, PLC$\beta$ is accumulated at the perisynaptic region and forms complexes coimmunoprecipitated with mGluR1$\alpha$, IP3R, and Shank (Nakamura et al., 2004; Hwang et al., 2005; Nomura et al., 2007). At excitatory synapses, group I mGluRs and their downstream molecules are thus physically interacted and recruited to the perisynaptic region, presumably to increase the efficiency and specificity of signal transduction. The same mechanism may recruit mGluR5 to the perisynaptic region of corticostriatal synapses (Paquet and Smith, 2003) (Fig. 4*A*) but might exclude $M_1$ from there (Fig. 4*B*). In contrast, mGluR5 is distributed more loosely around symmetrical synapses, regardless of synaptic and extrasynaptic membranes (Paquet and Smith, 2003) (our unpublished data). We assume that different somatodendritic and peri-

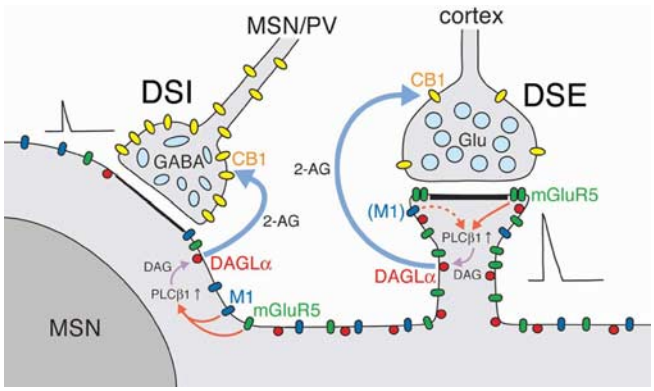


**Figure 10.** A schematic illustration showing the molecular, anatomical, and physiological organization of 2-AG-mediated retrograde signaling at excitatory (right) and inhibitory (left) synapses onto medium spiny neuron (MSN). At corticostriatal synapses, coincidental depolarization and mGluR5 activation are essential for PLC$\beta$1/DAGL$\alpha$-mediated production of 2-AG to induce DSE because of low $CB_1$ levels in excitatory corticostriatal afferents. Induction of mGluR5-assisted DSE is further facilitated with the aid of $M_1$, although $M_1$ activation alone cannot enhance DSE. This DSE facilitation mechanism will lead to the suppression of the hyperactivity of the MS neuron. At MSN–MSN and PV interneuron–MSN synapses, DSI can be induced by depolarization alone, attributable to high $CB_1$ levels in these inhibitory afferents. Nevertheless, coactivation of mGluR5 or $M_1$ robustly enhances the magnitude of DSI, which should lead to the increase of the excitability and striatal output of the MS neuron.

synaptic distributions between mGluR5 and $M_1$ (Fig. 10) may cause different extents of receptor–effector coupling and underlie differential effects of DHPG and oxo-M on DSE enhancement.

In conclusion, our findings provide evidence that a set of receptors and enzymes involved in 2-AG-mediated retrograde signaling are arranged in the striatum to be able to modulate effectively the excitability of the MS neuron depending on cortical activity and cholinergic tone.

## References


Aosaki T, Graybiel AM, Kimura M (1994) Effect of the nigrostriatal dopamine system on acquired neural responses in the striatum of behaving monkeys. Science 265:412–415.

Apicella P (2002) Tonically active neurons in the primate striatum and their role in the processing of information about motivationally relevant events. Eur J Neurosci 16:2017–2026.

Baude A, Nusser Z, Roberts JD, Mulvihill E, McIlhinney RA, Somogyi P (1993) The metabotropic glutamate receptor (mGluR1$\alpha$) is concentrated at perisynaptic membrane of neuronal subpopulations as detected by immunogold reaction. Neuron 11:771–787.

Bennett BD, Wilson CJ (1998) Synaptic regulation of action potential timing in neostriatal cholinergic interneurons. J Neurosci 18:8539–8549.

Bisogno T, Howell F, Williams G, Minassi A, Cascio MG, Ligresti A, Matias I, Schiano-Moriello A, Paul P, Williams EJ, Gangadharan U, Hobbs C, Di Marzo V, Doherty P (2003) Cloning of the first sn1-DAG lipases points to the spatial and temporal regulation of endocannabinoid signaling in the brain. J Cell Biol 163:463–468.

Bodor AL, Katona I, Nyiri G, Mackie K, Ledent C, Hajos N, Freund TF (2005) Endocannabinoid signaling in rat somatosensory cortex: laminar differences and involvement of specific interneuron types. J Neurosci 25:6845–6856.

Bolam JP, Hanley JJ, Booth PAC, Brevan MD (2000) Synaptic organization of the basal ganglia. J Anat 1196:527–542.

Brakeman PR, Lanahan AA, O'Brien R, Roche K, Barnes CA, Huganir RL, Worley PF (1997) Homer: a protein that selectively binds metabotropic glutamate receptors. Nature 386:284–288.

Brenowitz SD, Regehr WG (2003) Calcium dependence of retrograde inhibition by endocannabinoids at synapses onto Purkinje cells. J Neurosci 23:6373–6384.

Brenowitz SD, Regehr WG (2005) Associative short-term synaptic plasticity mediated by endocannabinoids. Neuron 45:419–431.

Chevaleyre V, Takahashi KA, Castillo PE (2006) Endocannabinoid-mediated synaptic plasticity in the CNS. Annu Rev Neurosci 29:37–76.

Deniau JM, Menetrey A, Charpier S (1996) The lamellar organization of the rat substantia nigra pars reticulata: segregated patterns of striatal afferents and relationship to the topography of corticostriatal projections. Neuroscience 73:761–781.

Dong H, O'Brien RJ, Fung ET, Lanahan AA, Worley PF, Huganir RL (1997) GRIP: a synaptic PDZ domain-containing protein that interacts with AMPA receptors. Nature 386:279–284.

Egertova M, Elphick MR (2000) Localisation of cannabinoid receptors in the rat brain using antibodies to the intracellular C-terminal tail of CB. J Comp Neurol 422:159–171.

Freiman I, Anton A, Monyer H, Urbanski MJ, Szabo B (2006) Analysis of the effects of cannabinoids on identified synaptic connections in the caudate-putamen by paired recordings in transgenic mice. J Physiol (Lond) 575:789–806.

Fujiyama F, Kuramoto E, Okamoto K, Hioki H, Furuta T, Zhou L, Nomura S, Kaneko T (2004) Presynaptic localization of an AMPA-type glutamate receptor in corticostriatal and thalamostriatal axon terminals. Eur J Neurosci 20:3322–3330.

Fukudome Y, Ohno-Shosaku T, Matsui M, Omori Y, Fukaya M, Tsubokawa H, Taketo MM, Watanabe M, Manabe T, Kano M (2004) Two distinct classes of muscarinic action on hippocampal inhibitory synapses: M2-mediated direct suppression and M1/M3-mediated indirect suppression through endocannabinoid signalling. Eur J Neurosci 19:2682–2692.

Fusco FR, Martorana A, Giampa C, De March Z, Farini D, D'Angelo V, Sancesario G, Bernardi G (2004) Immunolocalization of CB1 receptor in rat striatal neurons: a confocal microscopy study. Synapse 53:159–167.

Gerdeman G, Lovinger DM (2001) CB1 cannabinoid receptor inhibits synaptic release of glutamate in rat dorsolateral striatum. J Neurophysiol 85:468–471.

Gerdeman GL, Ronesi J, Lovinger DM (2002) Postsynaptic endocannabinoid release is critical to long-term depression in the striatum. Nat Neurosci 5:446–451.

Hajos N, Katona I, Naiem SS, MacKie K, Ledent C, Mody I, Freund TF (2000) Cannabinoids inhibit hippocampal GABAergic transmission and network oscillations. Eur J Neurosci 12:3239–3249.

Hashimotodani Y, Ohno-Shosaku T, Tsubokawa H, Ogata H, Emoto K, Maejima T, Araishi K, Shin HS, Kano M (2005) Phospholipase C$\beta$ serves as a coincidence detector through its $Ca^{2+}$ dependency for triggering retrograde endocannabinoid signal. Neuron 45:257–268.

Hashimotodani Y, Ohno-Shosaku T, Kano M (2007) Endocannabinoids and synaptic function in the CNS. Neuroscientist 27:1211–1219.

Herkenham M, Lynn AB, Johnson MR, Melvin LS, de Costa BR, Rice KC (1991) Characterization and localization of cannabinoid receptors in rat brain: a quantitative *in vitro* autoradiographic study. J Neurosci 11:563–583.

Hikosaka O, Wurtz RH (1989) The basal ganglia. Rev Oculomot Res 3:257–281.

Hohmann AG, Herkenham M (2000) Localization of cannabinoid CB(1) receptor mRNA in neuronal subpopulations of rat striatum: a double-label in situ hybridization study. Synapse 37:71–80.

Huang CC, Lo SW, Hsu KS (2001) Presynaptic mechanisms underlying cannabinoid inhibition of excitatory synaptic transmission in rat striatal neurons. J Physiol (Lond) 532:731–748.

Hwang JI, Kim HS, Lee JR, Kim E, Ryu SH, Suh PG (2005) The interaction of phospholipase C-$\beta$3 with Shank2 regulates mGluR-mediated calcium signal. J Biol Chem 280:12467–12473.

Julian MD, Martin AB, Cuellar B, Rodriguez De Fonseca F, Navarro M, Moratalla R, Garcia-Segura LM (2003) Neuroanatomical relationship between type 1 cannabinoid receptors and dopaminergic systems in the rat basal ganglia. Neuroscience 119:309–318.

Katona I, Sperlagh B, Sik A, Kafalvi A, Vizi ES, Mackie K, Freund TF (1999) Presynaptically located CB1 cannabinoid receptors regulate GABA release from axon terminals of specific hippocampal interneurons. J Neurosci 19:4544–4558.

Katona I, Rancz EA, Acsady L, Ledent C, Mackie K, Hajos N, Freund TF (2001) Distribution of CB1 cannabinoid receptors in the amygdala and their role in the control of GABAergic transmission. J Neurosci 21:9506–9518.

Katona I, Urban GM, Wallace M, Ledent C, Jung KM, Piomelli D, Mackie K,

Freund TF (2006) Molecular composition of the endocannabinoid system at glutamatergic synapses. J Neurosci 26:5628–5637.

Kawamura Y, Fukaya M, Maejima T, Yoshida T, Miura E, Watanabe M, Ohno-Shosaku T, Kano M (2006) CB1 is the major cannabinoid receptor at excitatory presynaptic site in the hippocampus and cerebellum. J Neurosci 26:2991–3001.

Kim J, Isokawa M, Ledent C, Alger BE (2002) Activation of muscarinic acetylcholine receptors enhances the release of endogenous cannabinoids in the hippocampus. J Neurosci 22:10182–10191.

Kita H, Kosaka T, Heizmann CW (1990) Parvalbumin-immunoreactive neurons in the rat neostriatum: a light and electron microscopic study. Brain Res 536:1–15.

Kofalvi A, Rodrigues RJ, Ledent C, Mackie K, Vizi ES, Cunha RA, Sperlagh B (2005) Involvement of cannabinoid receptors in the regulation of neurotransmitter release in the rodent striatum: a combined immunochemical and pharmacological analysis. J Neurosci 25:2874–2884.

Koos T, Tepper JM (1999) Inhibitory control of neostriatal projection neurons by GABAergic interneurons. Nat Neurosci 2:467–472.

Kreitzer AC, Malenka RC (2005) Dopamine modulation of state-dependent endocannabinoid release and long-term depression in the striatum. J Neurosci 25:10537–10545.

Kreitzer AC, Regehr WG (2001) Retrograde inhibition of presynaptic calcium influx by endogenous cannabinoids at excitatory synapses onto Purkinje cells. Neuron 29:717–727.

Kubota Y, Kawaguchi Y (2000) Dependence of GABAergic synaptic areas on the interneuron type and target size. J Neurosci 20:375–386.

Lujan R, Nusser Z, Roberts JD, Shigemoto R, Somogyi P (1996) Perisynaptic location of metabotropic glutamate receptors mGluR1 and mGluR5 on dendrites and dendritic spines in the rat hippocampus. Eur J Neurosci 8:1488–1500.

Lujan R, Roberts JD, Shigemoto R, Ohishi H, Somogyi P (1997) Differential plasma membrane distribution of metabotropic glutamate receptors mGluR1$\alpha$, mGluR2 and mGluR5, relative to neurotransmitter release sites. J Chem Neuroanat 13:219–241.

Maejima T, Hashimoto K, Yoshida T, Aiba A, Kano M (2001) Presynaptic inhibition caused by retrograde signal from metabotropic glutamate to cannabinoid receptors. Neuron 31:463–475.

Maejima T, Oka S, Hashimotodani Y, Ohno-Shosaku T, Aiba A, Wu D, Waku K, Sugiura T, Kano M (2005) Synaptically driven endocannabinoid release requires $Ca^{2+}$-assisted metabotropic glutamate receptor subtype 1 to phospholipase C$\beta$4 signaling cascade in the cerebellum. J Neurosci 25:6826–6835.

Marsicano G, Lutz B (1999) Expression of the cannabinoid receptor CB1 in distinct neuronal subpopulations in the adult mouse forebrain. Eur J Neurosci 11:4213–4225.

Matsuda LA, Bonner TI, Lolait SJ (1993) Localization of cannabinoid receptor mRNA in rat brain. J Comp Neurol 327:535–550.

Matyas F, Yanovsky Y, Mackie K, Kelsch W, Misgeld U, Freund TF (2006) Subcellular localization of type 1 cannabinoid receptors in the rat basal ganglia. Neuroscience 137:337–361.

Mechoulam R, Ben-Shabat S, Hanus L, Ligumsky M, Kaminski NE, Schatz AR, Gopher A, Almog S, Martin BR, Compton DR, Pertwee RG, Griffin G, Bayewitch M, Barg J, Vogel Z (1995) Identification of an endogenous 2-monoglyceride, present in canine gut, that binds to cannabinoid receptors. Biochem Pharmacol 50:83–90.

Melis M, Perra S, Muntoni AL, Pillolla G, Lutz B, Marsicano G, Di Marzo V, Gessa GL, Pistis M (2004) Prefrontal cortex stimulation induces 2-arachidonoyl-glycerol-mediated suppression of excitation in dopamine neurons. J Neurosci 24:10707–10715.

Mitrano DA, Smith Y (2007) Comparative analysis of the subcellular and subsynaptic localization of mGluR1a and mGluR5 metabotropic glutamate receptors in the shell and core of the nucleus accumbens in rat and monkey. J Comp Neurol 500:788–806.

Miura E, Fukaya M, Sato T, Sugihara K, Asano M, Yoshioka K, Watanabe M (2006) Expression and distribution of JNK/SAPK-associated scaffold protein JSAP1 in developing and adult mouse brain. J Neurochem 97:1431–1446.

Miyazaki T, Fukaya M, Shimizu H, Watanabe M (2003) Subtype switching of vesicular glutamate transporters at parallel fibre-Purkinje cell synapses in developing mouse cerebellum. Eur J Neurosci 17:2563–2572.

Nakamura M, Sato K, Fukaya M, Araishi K, Aiba A, Kano M, Watanabe M (2004) Signaling complex formation of phospholipase C$\beta$4 with metabotropic glutamate receptor type 1$\alpha$ and 1,4,5-trisphosphate receptor at the perisynapse and endoplasmic reticulum in the mouse brain. Eur J Neurosci 20:2929–2944.

Narushima M, Hashimoto K, Kano M (2006a) Endocannabinoid-mediated short-term suppression of excitatory synaptic transmission to medium spiny neurons in the striatum. Neurosci Res 54:159–164.

Narushima M, Uchigashima M, Hashimoto K, Watanabe M, Kano M (2006b) Depolarization-induced suppression of inhibition mediated by endocannabinoids at synapses from fast-spiking interneurons to medium spiny neurons in the striatum. Eur J Neurosci 24:2246–2252.

Narushima M, Uchigashima M, Fukaya M, Matsui M, Manabe T, Hashimoto K, Watanabe M, Kano M (2007) Tonic enhancement of endocannabinoid-mediated retrograde suppression of inhibition by cholinergic interneuron activity in the striatum. J Neurosci 27:496–506.

Nomura S, Fukaya M, Tsujioka T, Wu D, Watanabe M (2007) Phospholipase C$\beta$3 is distributed in both somatodendritic and axonal compartments and localized around perisynapse and smooth endoplasmic reticulum in mouse Purkinje cell subsets. Eur J Neurosci 25:659–672.

Nusser Z, Mulvihill E, Streit P, Somogyi P (1994) Subsynaptic segregation of metabotropic and ionotropic glutamate receptors as revealed by immunogold localization. Neuroscience 61:421–427.

Ohno-Shosaku T, Maejima T, Kano M (2001) Endogenous cannabinoids mediate retrograde signals from depolarized postsynaptic neurons to presynaptic terminals. Neuron 29:729–738.

Ohno-Shosaku T, Shosaku J, Tsubokawa H, Kano M (2002) Cooperative endocannabinoid production by neuronal depolarization and group I metabotropic glutamate receptor activation. Eur J Neurosci 15:953–961.

Ohno-Shosaku T, Matsui M, Fukudome Y, Shosaku J, Tsubokawa H, Taketo MM, Manabe T, Kano M (2003) Postsynaptic M1 and M3 receptors are responsible for the muscarinic enhancement of retrograde endocannabinoid signalling in the hippocampus. Eur J Neurosci 18:109–116.

Ohno-Shosaku T, Hashimotodani Y, Maejima T, Kano M (2005) Calcium signaling and synaptic modulation: regulation of endocannabinoid-mediated synaptic modulation by calcium. Cell Calcium 38:369–374.

Palomaki VA, Lehtonen M, Savinainen JR, Laitinen JT (2007) Visualization of 2-arachidonoylglycerol and cannabinoid CB(1) receptor activity in rat brain cryosections by functional autoradiography. J Neurochem, in press.

Paquet M, Smith Y (2003) Group I metabotropic glutamate receptors in the monkey striatum: subsynaptic association with glutamatergic and dopaminergic afferents. J Neurosci 23:7659–7669.

Piomelli D (2003) The molecular logic of endocannabinoid signalling. Nat Rev Neurosci 4:873–884.

Ramanathan S, Hanley JJ, Deniau JM, Bolam JP (2002) Synaptic convergence of motor and somatosensory cortical afferents onto GABAergic interneurons in the rat striatum. J Neurosci 22:8158–8169.

Robbe D, Kopf M, Remaury A, Bockaert J, Manzoni OJ (2002) Endogenous cannabinoids mediate long-term synaptic depression in the nucleus accumbens. Proc Natl Acad Sci USA 99:8384–8388.

Ronesi J, Lovinger DM (2005) Induction of striatal long-term synaptic depression by moderate frequency activation of cortical afferents in rat. J Physiol (Lond) 562:245–256.

Ronesi J, Gerdeman GL, Lovinger DM (2004) Disruption of endocannabinoid release and striatal long-term depression by postsynaptic blockade of endocannabinoid membrane transport. J Neurosci 24:1673–1679.

Safo PK, Regehr WG (2005) Endocannabinoids control the induction of cerebellar LTD. Neuron 48:647–659.

Sheng M, Kim E (2000) The Shank family of scaffold proteins. J Cell Sci 113:1851–1856.

Somogyi J, Baude A, Omori Y, Shimizu H, El Mestikawy S, Fukaya M, Shigemoto R, Watanabe M, Somogyi P (2004) GABAergic basket cells expressing cholecystokinin contain vesicular glutamate transporter type 3 (VGLUT3) in their synaptic terminals in hippocampus and isocortex of the rat. Eur J Neurosci 19:552–569.

Stella N, Schweitzer P, Piomelli D (1997) A second endogenous cannabinoid that modulates long-term potentiation. Nature 388:773–778.

Sugiura T, Kondo S, Sukagawa A, Nakane S, Shinoda A, Itoh K, Yamashita A, Waku K (1995) 2-Arachidonoylglycerol: a possible endogenous cannabinoid receptor ligand in brain. Biochem Biophys Res Commun 215:89–97.

Szabo B, Dorner L, Pfreundtner C, Norenberg W, Starke K (1998) Inhibition of GABAergic inhibitory postsynaptic currents by cannabinoids in rat corpus striatum. Neuroscience 85:395–403.

Szabo B, Urbanski MJ, Bisogno T, Di Marzo V, Mendiguren A, Baer WU, Freiman I (2006) Depolarization-induced retrograde synaptic inhibition in the mouse cerebellar cortex is mediated by 2-arachidonoylglycerol. J Physiol 577:263–280.

Tanaka J, Nakagawa S, Kushiya E, Yamasaki M, Fukaya M, Iwanaga T, Simon MI, Sakimura K, Kano M, Watanabe M (2000) Gq protein alpha subunits Gαq and Gα11 are localized at postsynaptic extra-junctional membrane of cerebellar Purkinje cells and hippocampal pyramidal cells. Eur J Neurosci 12:781–792.

Tepper JM, Bolam JP (2004) Functional diversity and specificity of neostriatal interneurons. Curr Opin Neurobiol 14:685–692.

Tepper JM, Koos T, Wilson CJ (2004) GABAergic microcircuits in the neostriatum. Trends Neurosci 27:662–669.

Tu JC, Xiao B, Yuan JP, Lanahan AA, Leoffert K, Li M, Linden DJ, Worley PF (1998) Homer binds a novel proline-rich motif and links group 1 metabotropic glutamate receptors with IP3 receptors. Neuron 21:717–726.

Uemura T, Mori H, Mishina M (2004) Direct interaction of GluRδ2 with Shank scaffold proteins in cerebellar Purkinje cells. Mol Cell Neurosci 26:330–341.

Varma N, Carlson GC, Ledent C, Alger BE (2001) Metabotropic glutamate receptors drive the endocannabinoid system in hippocampus. J Neurosci 21:RC188(1–5).

Wang Z, Kai L, Day M, Ronesi J, Yin HH, Ding J, Tkatch T, Lovinger DM, Surmeier DJ (2006) Dopaminergic control of corticostriatal long-term synaptic depression in medium spiny neurons is mediated by cholinergic interneurons. Neuron 50:443–452.

Watanabe K, Kimura M (1998) Dopamine receptor-mediated mechanisms involved in the expression of learned activity of primate striatal neurons. J Neurophysiol 79:2568–2580.

Watanabe M, Nakamura M, Sato K, Kano M, Simon MI, Inoue Y (1998) Patterns of expression for the mRNA corresponding to the four isoforms of phospholipase Cβ in mouse brain. Eur J Neurosci 10:2016–2025.

Wilson CJ (2004) Basal ganglia. In: The synaptic organization of the brain, Ed 5 (Shephard GM, ed), pp361–414. Oxford: Oxford UP.

Wilson RI, Nicoll RA (2001) Endogenous cannabinoids mediate retrograde signalling at hippocampal synapses. Nature 410:588–592.

Yamada K, Fukaya M, Shimizu H, Sakimura K, Watanabe M (2001) NMDA receptor subunits GluRε1, GluRε3 and GluRζ1 are enriched at the mossy fibre-granule cell synapse in the adult mouse cerebellum. Eur J Neurosci 13:2025–2036.

Yan Z, Flores-Hernandez J, Surmeier DJ (2001) Coordinated expression of muscarinic receptor messenger RNAs in striatal medium spiny neurons. Neuroscience 103:1017–1024.

Yin HH, Lovinger DM (2006) Frequency-specific and D2 receptor-mediated inhibition of glutamate release by retrograde endocannabinoid signaling. Proc Natl Acad Sci USA 103:8251–8256.

Yoshida T, Fukaya M, Uchigashima M, Miura E, Kamiya H, Kano M, Watanabe M (2006) Localization of diacylglycerol lipase-α around postsynaptic spine suggests close proximity between production site of an endocannabinoid, 2-arachidonoyl-glycerol, and presynaptic cannabinoid CB1 receptor. J Neurosci 26:4740–4751.

Zimmer A, Zimmer AM, Hohmann AG, Herkenham M, Bonner TI (1999) Increased mortality, hypoactivity, and hypoalgesia in cannabinoid CB1 receptor knockout mice. Proc Natl Acad Sci USA 96:5780–5785.